JACS
JOURNAL OF THE AMERICAN CHEMICAL SOCIETY
Article
Cite This: J. Am. Chem. Soc. 2020, 142, 633−640
pubs.acs.org/JACS

Selective Ethane/Ethylene Separation in a Robust Microporous Hydrogen-Bonded Organic Framework

Xu Zhang,[†,‡] Libo Li,[§,∥] Jia-Xin Wang,[†] Hui-Min Wen,[⊥] Rajamani Krishna,[#] Hui Wu,[▽] Wei Zhou,[▽] Zhong-Ning Chen,[‡] Bin Li,*[,†] Guodong Qian,[†] and Banglin Chen*[,∥]

[†]State Key Laboratory of Silicon Materials, School of Materials Science and Engineering, Zhejiang University, Hangzhou 310027, China

[‡]State Key Laboratory of Structural Chemistry, Fujian Institute of Research on the Structure of Matter, Chinese Academy of Sciences, Fuzhou, Fujian 350002, China

[§]College of Chemistry and Chemical Engineering, Shanxi Key Laboratory of Gas Energy Efficient and Clean Utilization, Taiyuan University of Technology, Taiyuan 030024, Shanxi, China

[∥]Department of Chemistry, University of Texas at San Antonio, One UTSA Circle, San Antonio, Texas 78249-0698, United States

[⊥]College of Chemical Engineering, Zhejiang University of Technology, Zhejiang 310014, P. R. China

[#]Van 't Hoff Institute for Molecular Sciences, University of Amsterdam, Science Park 904, 1098 XH Amsterdam, The Netherlands

[▽]NIST Center for Neutron Research, National Institute of Standards and Technology, Gaithersburg, Maryland 20899-6102, United States

Supporting Information

ABSTRACT: The separation of ethane (C_2H_6) from ethylene (C_2H_4) is of prime importance in the production of polymer-grade C_2H_4 for industrial manufacturing. It is very challenging and still remains unexploited to fully realize efficient C_2H_6/C_2H_4 separation in the emerging hydrogen-bonded organic frameworks (HOFs) due to the weak nature of hydrogen bonds. We herein report the benchmark example of a novel ultrarobust HOF adsorbent (termed as HOF-76a) with a Brunauer−Emmett−Teller surface area exceeding 1100 $m^2\ g^{-1}$, exhibiting the preferential binding of C_2H_6 over C_2H_4 and thus highly selective separation of C_2H_6/C_2H_4. Theoretical calculations indicate the key role of the nonpolar surface and the suitable triangular channel-like pores in HOF-76a to sterically "match" better with the nonplanar C_2H_6 molecule than the planar C_2H_4, thus affording overall stronger multipoint van der Waals interactions with C_2H_6. The exceptional separation performance of HOF-76a for C_2H_6/C_2H_4 separation was clearly demonstrated by gas adsorption isotherms, ideal adsorbed solution theory calculations, and simulated and experimental breakthrough curves. Breakthrough experiments on HOF-76a reveal that polymer-grade ethylene gas can be straightforwardly produced from 50/50 (v/v) C_2H_6/C_2H_4 mixtures during the first adsorption cycle with a high productivity of 7.2 L/kg at 298 K and 1.01 bar and 18.8 L/kg at 298 K and 5.0 bar, respectively.

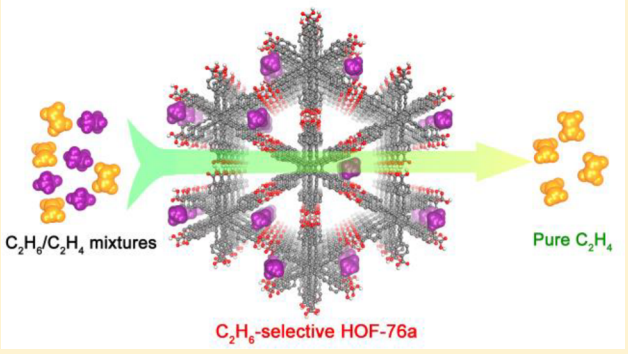

INTRODUCTION

Ethylene (C_2H_4) is one of the most important feedstocks in petrochemical industries with a global production capacity of exceeding 170 million tons per year, and is mostly produced by steam cracking of ethane (C_2H_6) and liquefied petroleum gas.[1,2] Steam crackers inevitably yield many other hydrocarbons (mostly C_2H_6) that must be removed for polymer production. The purity of ethylene thereby primarily depends on the removal of ethane; this separation process is energy-intensive and conventionally dominated by the cryogenic distillation because of the close physicochemical properties of the two components. The total energy used for purification of ethylene and propene even accounts for 0.3% of global energy consumption, highlighting as one of the most important industrial separation tasks.[3]

Adsorbent-based gas separation has been considered as a viable alternative to replace traditional cryogenic distillation processes.[4] Development of C_2H_6-selective adsorbents is more desired for C_2H_4/C_2H_6 separation because pure C_2H_4 can be directly produced during the adsorption cycle, avoiding an additional C_2H_4 desorption step and subsequent multiple adsorption−desorption purification cycles of C_2H_4-selective materials and thus simplifying the separation process with

Received: November 18, 2019
Published: December 14, 2019

DOI: 10.1021/jacs.9b12428
J. Am. Chem. Soc. 2020, 142, 633−640

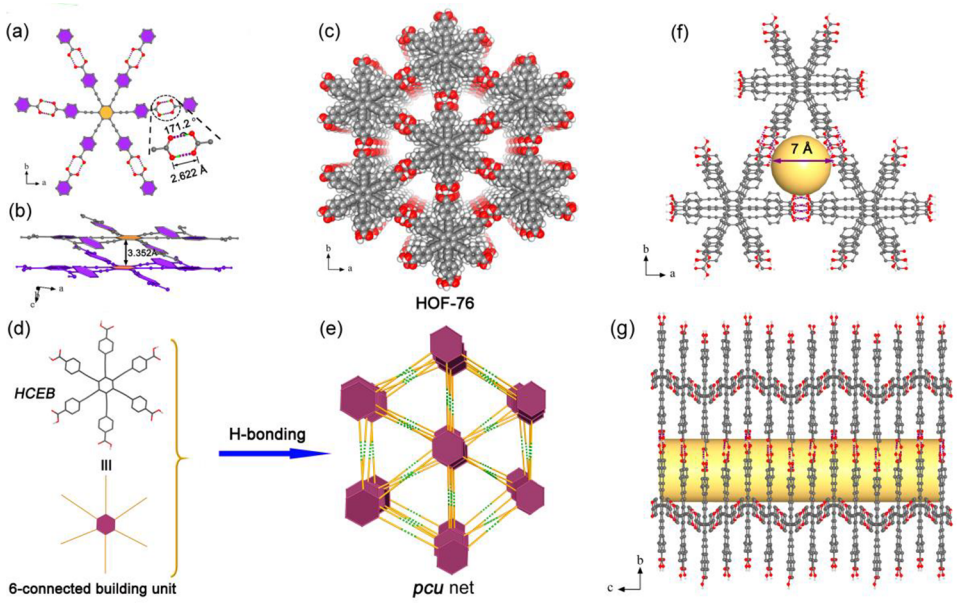

Figure 1. Crystal structure description of HOF-76. (a) View of the connection of adjacent building blocks and the associated hydrogen-bond length and angle. (b) Strong face-to-face $\pi-\pi$ stacking interactions. (c) Representation of the porous framework of HOF-76. (d) The structure of HCEB as six-connected nodes and (e) pcu-net (green dotted lines represent H-bonds). (g) One-dimensional (1D) triangular channels viewed along *c*-axis and (f) *a*-axis, revealing a moderate size of 7.0 Å in diameter.

remarkable energy saving. However, most of developed adsorbents, such as metal-containing alumina, carbons, zeolites, and metal−organic frameworks (MOFs), commonly take up more amounts of C_2H_4 than C_2H_6.[5−8] This is because the C_2H_4 molecule has a larger quadrupole moment (C_2H_4: 1.50×10^{-26} esu cm^2, C_2H_6: 0.65×10^{-26} esu cm^2) and the presence of π electrons,[9] rendering its stronger interactions with metal sites/clusters. Conversely, ethane has a higher polarizability than ethylene (44.7×10^{-25} vs 42.52×10^{-25} cm^3); so C_2H_6-selective adsorbents prefer to possess a pore structure enriched with nonpolar/inert surfaces (e.g., featuring aromatic or aliphatic moieties), wherein dispersion and induction interactions can make major contributions.[10] In this regard, inorganic secondary building units (SBUs) in MOFs are commonly detrimental to building nonpolar/inert surfaces,[11] making most of them absorb more C_2H_4 over C_2H_6. To date, only a handful of C_2H_6-selective MOFs have been fulfilled by incorporating the well-designed C_2H_6-affinity sites or inert pore surfaces.[12−17]

Realization of new class of adsorbents that are easy to build nonpolar/inert surfaces is of great importance to target the looked-for C_2H_6-selective adsorbents. In this context, hydrogen-bonded organic frameworks (HOFs), as a new type of extended porous materials, come into our sight because they can be self-assembled from organic molecules via intermolecular hydrogen-bonding interactions.[18] The metal-free nature without highly polar groups endows the pores of HOFs natively enriched with the nonpolar/inert surfaces that might lead to some new C_2H_6-selective adsorbents. Unlike the well-established MOFs and covalent organic frameworks (COFs) that are connected by strong coordinative or covalent bonds, HOFs are constructed by weak hydrogen-bonding interactions that make the framework very difficult to stabilize, and most of them collapse upon removal of solvent molecules by thermal and/or vacuum activation. This drawback led to the first establishment of permanent porosity in HOFs until 2010.[18,19] Evidently, the research of the emerging porous HOFs is still in its comparatively early stage when compared with MOFs and COFs. However, the soft nature of hydrogen bonding endows HOFs with some unique advantages, such as high solution processability and characterization, easy purification, good thermal stability, and facile regeneration and reusage by simple recrystallization.[20−22] Despite these attractive merits, it is still very challenging to obtain robust HOFs with precise crystal structure, large permanent porosity, and both chemical and thermal stability, which largely hampers its development for gas separation. Until now, no efficient C_2H_6-selective HOF adsorbents have been fully realized for the important and challenging C_2H_6/C_2H_4 separation.

With the above consideration in mind, we reasoned that constructing the nonpolar/inert pore surfaces within robust HOF materials may lead to the desired C_2H_6-selective adsorbents but remains a challenge. We herein designed a C_6-symmetry organic ligand hexakis(4-carboxyphenylethynyl)-benzene (HCEB) with large π-conjugated system and six carboxylate acid groups (Figure 1) and used it as a building unit to construct a novel robust HOF adsorbent (HOF-76). Single-crystal X-ray structure determination revealed that the synergistic effect of high density of strong O−H···O hydrogen bonds and the consecutive strong $\pi\cdots\pi$ interactions in HOF-76 guarantees the establishment of permanent porosity with a Brunauer−Emmett−Teller (BET) surface area of 1121 m^2 g^{-1} and afford its highly thermal and chemical stabilities. As expected, we discovered, for the first time, that the nonpolar/inert pore surfaces within the activated HOF-76a indeed lead to the preferential adsorption of C_2H_6 over C_2H_4, and the separation performance is better than most of MOF materials reported. Simulated and actual breakthrough experiments confirmed that HOF-76a can preferentially capture C_2H_6 from C_2H_6/C_2H_4 mixtures to directly produce high-purity C_2H_4 gas with a high productivity of 7.2 L/kg at 298 K and 1.01 bar and 18.8 L/kg at 5 bar and 298 K, a value comparable to the record 19.3 L/kg in $Fe_2(O_2)(dobdc)$,[13] opening a new

DOI: 10.1021/jacs.9b12428
J. Am. Chem. Soc. 2020, 142, 633−640

class of porous adsorbents for the challenging C_2H_6/C_2H_4 separation.

EXPERIMENTAL SECTION

Materials and Physical Measurements. All starting chemicals and solvents were purchased from commercial companies and used without further purification. ^1H and ^{13}C NMR spectra were recorded on Bruker AVANCE III spectrometers (400 MHz; Figure S1–S4). Thermogravimetric analysis (TGA) was performed on a Netzsch STA 449C thermal analyzer from 30 to 800 °C under nitrogen atmosphere at a heating rate of 5 °C/min. Powder X-ray diffraction (PXRD) patterns were measured by a BRUKER D8 ADVANCE diffractometer employing Cu K radiation operated at 30 kV and 15 mA, scanning over the range 2–45° (2θ) at a rate of 2°/min. Compound **1** and HCEB were prepared according to the literature with slight modification.[23]

Synthesis of Hexakis(4-ethoxycarbonylphenylethynyl)-benzene (1). Under an argon atmosphere, hexabromobenzene (551 mg, 1.0 mmol), ethyl 4-ethynylbenzoate (1.39 g, 8.0 mmol), $Pd(PPh_3)_2Cl_2$ (126 mg, 0.18 mmol), CuI (69 mg, 0.36 mmol), PPh_3 (94 mg, 0.36 mmol), and degassed Et_3N (50 mL) were combined in a 100 mL two neck round-bottom flask. This mixture was stirred at refluxing temperature for 48 h. After removal of organic solvent, the crude product was purified by column chromatography on silica gel with CH_2Cl_2/ethyl acetate (EA; 1:1 v/v) to give the pure product **1** as a yellow solid. Yield: 832 mg, 75%. ^1H NMR ($CDCl_3$, 400 MHz, ppm): δ 7.92 (d, J = 7.08 Hz, 12H), 7.51 (d, J = 7.04 Hz, 12H), 4.40 (q, J = 7.12 Hz, 12H), 1.44 (t, J = 7.16 Hz, 18H). ^{13}C NMR ($CDCl_3$, ppm): δ 165.8, 131.7, 130.8, 129.7, 127.8, 127.2, 99.3, 89.5, 61.5, 14.5.

Synthesis of Hexakis(4-carboxyphenylethynyl)benzene ligand (HCEB). A solution of compound **1** (800 mg, 0.72 mmol) in THF (60 mL) was added to a 60 mL water solution of KOH (3.36 g, 60 mmol). The suspension mixture was stirred at 70 °C for 48 h. After removal of organic solvent, the aqueous residue was acidified with 2 M HCl. The resulting precipitate was filtered, washed with water, and dried under vacuum to afford HCEB as a dark yellow solid. Yield: 625 mg, 92%. ^1H NMR (DMSO-d_6, 400 MHz, ppm): δ 13.01 (s, 6H), 7.57 (d, J = 7.40 Hz, 12H), 7.20 (d, J = 7.40 Hz, 12H). ^{13}C NMR (DMSO-d_6, ppm): δ 166.3, 131.2, 130.9, 129.1, 126.9, 125.9, 98.8, 89.0.

Synthesis of HOF-76. The 50 mg of HCEB ligand was dissolved in a solution of DMSO (15 mL) in a 50 mL beaker, which was put in a 250 mL sealed beaker with 100 mL of acetone. The yellow needle crystals of HOF-76 suitable for single crystal X-ray diffraction analysis were grown by vapor diffusion for several weeks at room temperature. Yield: 45 mg, 90%.

Single-Crystal X-ray Crystallography. Single-crystal X-ray diffraction data of HOF-76 was collected on a Bruker D8 VENTURE diffractometer at 100 K using graphite-monochromated Mo Ka (λ = 0.71073 Å) radiation. The structure was solved by direct method and refined on F^2 by full-matrix least-squares methods using SHELXL-97 software package.[24] The solvate molecules of all data were treated as diffuse contribution to the overall scattering without specific atom positions by SQUEEZE/PLATON due to severe disorder of these solvate molecules in the lattices.[25] The crystal data are summarized in Table S3.

Density Functional Theory Calculations. Our first-principles density-functional theory (DFT) calculations were performed using the Quantum-Espresso package.[26] A semiempirical addition of dispersive forces to conventional DFT[27] was included in the calculation to account for van der Waals interactions. We used Vanderbilt-type ultrasoft pseudopotentials and the generalized gradient approximation (GGA) with the Perdew–Burke–Ernzerhof (PBE) exchange correlation. We first fully optimized the bare HOF-76a structure, using the primitive unit cell. Then, C_2H_6 or C_2H_4 molecules were introduced into the triangular channel-like pores of HOF-76a, and structural relaxations were performed. Various gas adsorption positions and molecular orientations were examined to find the lowest energy configuration. To obtain the gas binding energies, a single gas molecule placed in a supercell with the same cell dimensions was also relaxed as a reference. The static binding energy (at T = 0 K) was calculated using $E_B = E_{(HOF\text{-}76a)} + E_{(gas)} - E_{(HOF\text{-}76a+gas)}$.

Gas Sorption Measurements. A Micromeritics ASAP 2020 surface area analyzer was used to measure gas adsorption isotherms. To remove all the guest solvents in the framework, the fresh crystal samples were first solvent-exchanged with dry acetone at least 10 times within 2 days, and evacuated at 273 K for 24 h and then 296 K for about 8 h until the outgas rate was 5 mmHg min^{-1} to yield the activated samples. The sorption measurement was maintained at 77 K under liquid nitrogen bath. Bath temperatures of 273 and 296 K were precisely controlled with a recirculating control system.

Column Breakthrough Experiments. The breakthrough experiments for C_2H_6/C_2H_4 (50/50, v/v), C_2H_6/C_2H_4 (10/90), and $C_2H_6/C_2H_4/CH_4/H_2/C_2H_2$ (10/87/1/1/1) mixtures were carried out at a flow rate of 1.25 mL/min (298 K, 1.01 or 5.0 bar). Activated HOF-76a powder samples (1.1 g) were packed into Φ 4 × 150 mm stainless steel column under pure N_2 atmosphere. The sample in each column was compressed as much as possible to obtain the best separation performance, and column voidages are similar for different samples. The horizontal reactor was placed in a temperature controlled environment, maintained at 298 K. The flow rates of all gases mixtures were regulated by mass flow controllers, and the effluent gas stream from the column is monitored by gas chromatography. Prior to breakthrough experiment, the sample was activated by flushing the adsorption bed with helium (He) gas for 2 h at 323 K. The adsorption bed can be regenerated by He flow (100 mL/min) for 1 h at 298 K.

RESULTS AND DISCUSSION

The ligand HCEB was readily synthesized on a gram scale using Sonogashira coupling of hexabromobenzene with ethyl 4-ethynylbenzoate, followed by hydrolysis and acidification (Scheme 1). Slow evaporation of an acetone solution into a

Scheme 1. Synthetic Routes to the Organic Building Block of HCEB

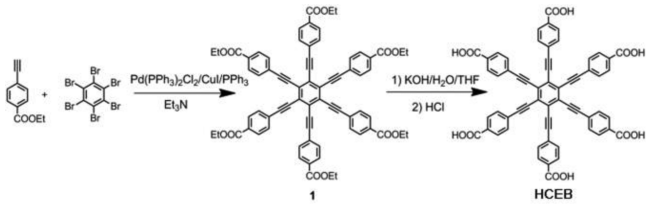

DMSO solution of HCEB produced HOF-76 as yellow needle crystals suitable for X-ray analysis. The phase purity of the bulk material was confirmed by matching the experimental and simulated powder X-ray diffraction patterns (PXRD; Figure S5).

Single crystal X-ray diffraction (XRD) analysis revealed that HOF-76 crystallizes in a monoclinic $C2/c$ space group with a hydrogen-bonded three-dimensional (3D) network (Table S3). As shown in Figure 1a, each HCEB molecule in HOF-76 is connected with six neighboring molecules through six pairs of O–H···O hydrogen bonds (H-bonds). The O–H···O distance and angle are 2.622 Å and 171.2°, respectively, which are typical for strong H-bonds with high directionality.[18] Since HCEB molecule has six carboxylate acid units, the density of H-bonds in HOF-76 can reach 6.276 mmol/cc, notably higher than those of robust carboxylic acid-type HOFs reported (Table S4). It is worthy of note that HCEB molecule is not flat but has a twisted conformation, in which two outer carboxyphenyl groups are on the same plane with the central benzene ring, while the other four groups alternately direct up

DOI: 10.1021/jacs.9b12428
J. Am. Chem. Soc. 2020, 142, 633–640

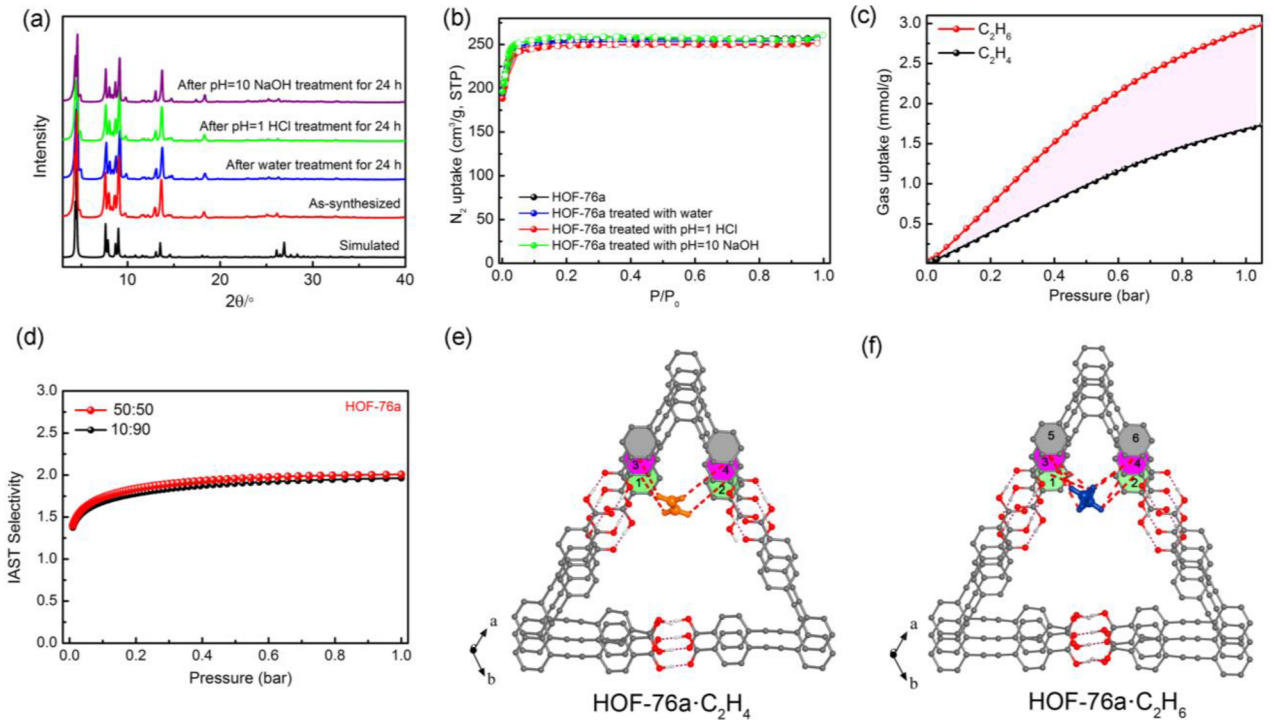

Figure 2. (a) PXRD patterns and (b) N_2 adsorption isotherms (77 K) of HOF-76a and the samples treated with water, HCl (pH 1) and NaOH (pH 10) solution, respectively. (c) Adsorption isotherms of C_2H_6 (red) and C_2H_4 (black) for HOF-76a at 296 K. (d) IAST selectivity of HOF-76a from C_2H_6/C_2H_4 (50/50 and 10/90) gas mixtures. (e and f) Comparison of the preferential C_2H_4 and C_2H_6 adsorption sites and the close vdW contacts within the corner surface of triangular channel-like pores observed by DFT calculations (C, dark gray; O, red; H, white), highlighting the C−H···π interactions in red dashed bonds.

and down with an angle of 20.3−22.6° against the central benzene ring (Figure S6). These structural features enable HCEB to construct a three-dimensionally extended H-bonded network (Figures 1c and S7). The center and outer phenyl rings along with six alkynyls in HCEB form a very large π-conjugated system. The distance between two adjacent π-conjugated systems is about 3.352 Å (Figure 1b), indicating a very strong face-to-face $\pi\cdots\pi$ stacking interaction. Topologically, if the HCEB is considered as a six-connected node, HOF-76 possesses the *pcu* $\{4^{12}6^3\}$ topology (Figure 1d,e). As shown in Figure 1f,g, HOF-76 exhibits a 1D triangular channel-like pore with a moderate size of 7.0 Å in diameter along the *c* axis. Due to the absence of metal sites/clusters, the channel surfaces are natively enriched with inert aromatic rings that may hold the potential to result in the preferential binding of C_2H_6 over C_2H_4.

Before evaluating gas sorption properties of HOF-76, we first investigated its thermal and chemical stabilities by PXRD patterns and thermogravimetric analysis (TGA). The foregoing structural studies clearly showed that HOF-76 has extremely high density of H-bonds, short O−H···O distance, and very strong $\pi\cdots\pi$ interactions (Table S4), which may contribute to high stabilities. As depicted in Figure 2a, HOF-76 indeed exhibits highly thermal and chemical stabilities. The framework can retain its structural integrity without phase change observed after soaking the sample in water, HCl (pH 1) and NaOH (pH 10) solutions for 24 h. There is also no loss of crystallinity when the sample was exposed to air for over 2 months (Figure S8). Along with the stability to water, the thermal stability of HOF-76 is also worthy of being examined. TGA studies revealed that HOF-76a is thermally stable up to 350 °C in an N_2 atmosphere (Figure S9). No obvious phase changes in the PXRD patterns could be observed even at 300 °C in an air atmosphere, as evidence by various temperature PXRD patterns (Figure S10).

The permanent porosity of the activated HOF-76a was confirmed by nitrogen (N_2) gas sorption experiments at 77 K. As shown in Figure 2b, HOF-76a takes up 258 $cm^3\ g^{-1}$ N_2 at 77 K and 1 bar, and the N_2 isotherm shows a significant type I sorption behavior without any hysteresis, characteristic of microporous materials. The BET surface area and pore volume of HOF-76a were calculated to be 1121 $m^2\ g^{-1}$ and 0.40 $cm^3\ g^{-1}$ (Figure S12). The pore size distribution determined by N_2 isotherms is shown in Figure S13, and the calculated pore size (8.5 Å) is close to the value (7.0 Å) obtained from the crystal structure. After heating at 300 °C for 2 h or immersing in water, HCl and NaOH solutions for 24 h, the reactivated HOF-76a samples show no obvious decrease on the N_2 uptakes at 77 K compared with the pristine sample, further confirming its excellent chemical and thermal stabilities.

Establishment of the permanent porosity in robust HOF-76a prompted us to examine the single-component adsorption isotherms of C_2H_6 and C_2H_4 at 273 and 296 K up to 1 bar, respectively. As depicted in Figures 2c and S14, HOF-76a shows an obviously preferential adsorption of C_2H_6 over C_2H_4 at both temperatures. The C_2H_6 uptake amount of HOF-76a (2.95 mmol g^{-1}) is much higher than that of C_2H_4 (1.67 mmol g^{-1}) at 1 bar and 296 K, affording a large C_2H_6/C_2H_4 uptake ratio of 177%. Thus, we successfully realized the "reversed C_2H_6/C_2H_4 adsorption" in HOF-76a. The adsorption heat (Q_{st}) of C_2H_6 for HOF-76a was calculated to be ~22.8 kJ/mol at zero coverage, slightly higher than that of C_2H_4 (Figure S16). Due to the absence of metal sites/clusters and polar binding sites, this Q_{st} value of C_2H_6 is significantly lower than

DOI: 10.1021/jacs.9b12428
J. Am. Chem. Soc. 2020, 142, 633−640

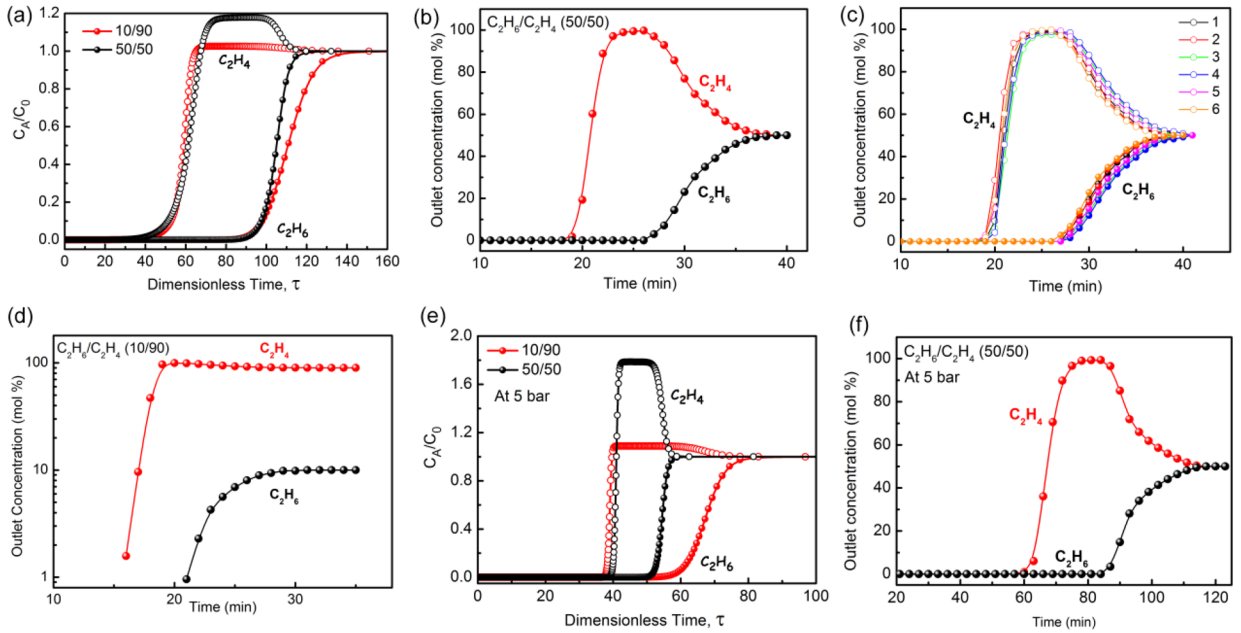

Figure 3. (a) Simulated breakthrough curves for C_2H_6/C_2H_4 (50/50 and 10/90) separation (C_A/C_0, outlet concentration/feed concentration). (b) Experimental column breakthrough curves for a C_2H_6/C_2H_4 (50/50) mixture in an absorber bed packed with HOF-76a at 298 K and 1.01 bar. (c) The recyclability of HOF-76a under multiple mixed-gas column breakthrough tests. (d) Experimental breakthrough curves for a C_2H_6/C_2H_4 (10/90) mixture. (e) Simulated breakthrough curves for C_2H_6/C_2H_4 mixtures at 5 bar. (f) Experimental breakthrough curves for a C_2H_6/C_2H_4 (50/50) mixture at 298 K and 5 bar.

that in most of the C_2H_6-selective MOFs, such as MAF-49 (61 kJ/mol)[12] and $Fe_2(O_2)$(dobdc) (66.8 kJ/mol).[13]

Ideal adsorbed solution theory (IAST) was used to calculate the adsorption selectivity of HOF-76a for 50/50 and 10/90 C_2H_6/C_2H_4 mixtures at room temperature (RT), respectively. As shown in Figure 2d, HOF-76a exhibits a high C_2H_6/C_2H_4 selectivity of up to 2.0 for both gas mixtures, which is larger than most of the developed MOF materials and HOF-BTB (1.4),[20d] and only lower than $Fe_2(O_2)$(dobdc),[13] $Cu(Qc)_2$,[15] MAF-49,[12] and UiO-66−$2CF_3$[17a] (Figure S18 and Table S5). Further, the C_2H_6/C_2H_4 uptake ratio (177%) of HOF-76a at 1 bar outperforms almost all of the reported C_2H_6-selective materials except $Cu(Qc)_2$ (Figure S18), further confirming its exceptional selectivity. The C_2H_6 uptake of HOF-76a (2.95 mmol/g) at 1 bar and RT is also notably higher than those of benchmark UiO-66−$2CF_3$ (0.86 mmol/g),[17a] $Cu(Qc)_2$ (1.85 mmol/g),[15] and MAF-49 (1.73 mmol/g).[12] Overall, these results indicate that HOF-76a is placed among the best performing C_2H_6-selective materials reported. It is needed to point out that HOFs are a new kind of porous materials, and the research of porous HOFs for gas separation is still in its early stage. The development of robust HOF materials for C_2H_6/C_2H_4 separation is much more challenging than the well-established MOFs at this stage. However, HOFs hold some unique advantages that are different from MOFs, such as the ease of building nonpolar pores, solution processability and characterization, easy purification, and straightforward regeneration and reusage by simple recrystallization. These advantages make the pursuit of porous HOFs as separating adsorbents very attractive and become mutually complementary to the existing MOFs for the potential practical applications. In addition, HOF-76 also possesses ultrahigh chemical/thermal stabilities that are commonly absent in most C_2H_6-selective MOFs.

To gain better insight into the role of the nonpolar pore surface on the selective C_2H_6/C_2H_4 adsorption in HOF-76a, we performed calculations using first-principles dispersion-corrected density functional theory (DFT-D) method. We found that, for both C_2H_4 and C_2H_6 molecules, the primary adsorption sites are located at the corners of the triangular channel-like pores. The lowest-energy gas binding configurations are shown in Figure 2e,f. For clarity, we only showed one adsorbed gas molecule at the corner site. Within each unit cell, there exist 24 such "corner sites", which are crystallographically equivalent (Figure S19). The corresponding calculated static binding energies of C_2H_6 and C_2H_4 are 33.6 and 29.3 kJ mol^{-1}, respectively. Along the channel axis, the binding energy variation is small (within ~5 kJ mol^{-1}). As expected, the interaction between the gas molecule and the nonpolar pore surface is of van der Waals type, and the gas binding strength is modest. Nevertheless, the binding of C_2H_6 is still notably stronger than C_2H_4. This is partly because the nonplanar C_2H_6 molecule sterically "matches" better to the corner surface of the triangular channel-like pore than the planar C_2H_4 molecule. As a result, multiple C−H···π interactions exist between the C_2H_6 molecule and phenyl rings (Figures 2e and S20), in which all six hydrogens of C_2H_6 can interact with six adjacent phenyl rings 1−6 and the H···π distances are calculated to be 4.116−4.857 Å. In contrast, the C_2H_4 molecule shows contacts only with four phenyl rings 1−4 with the longer H···π distances of 4.372−5.046 Å. Thus, the lower binding energy of C_2H_4 can be attributed to the lack of strong permanent dipoles on the nonpolar pore surface of HOF framework and the less number of C−H···π interactions. Accordingly, for ethane, the more C−H···π interactions and its higher polarizability indicate the higher binding affinity. This is fully consistent with our experimental observations (Q_{st} etc.). In addition, we note that a full occupancy of these corner sites would correspond to 3.2 mmol/g gas uptake, which is close to

DOI: 10.1021/jacs.9b12428
J. Am. Chem. Soc. 2020, 142, 633−640

the experimental C_2H_6 uptake (2.95 mmol/g) at RT and 1 bar, indicating that the corner sites are heavily populated. In contrast, for C_2H_4, the uptake at RT and 1 bar is much lower (1.67 mmol/g), suggesting that only about half of the corner sites are populated due to its weaker binding affinity and worse sterical "match" with the pores. All of these results can explain the adsorption/separation mechanisms at 1 bar qualitatively.

Transient breakthrough simulations were first performed for HOF-76a in fixed-bed adsorption processes at 1 bar and 298 K to determine the feasibility of C_2H_6/C_2H_4 separation. As shown in Figure 3a, efficient separations can be accomplished by HOF-76a for both of C_2H_6/C_2H_4 gas mixtures (50/50 and 10/90), wherein C_2H_4 breakthrough occurred first and C_2H_6 passed through the fixed bed after a certain time (τ_{break}). Next, the experimental breakthrough studies were conducted in a packed column of HOF-76a under actual C_2H_6/C_2H_4 (50/50) mixtures at 298 K. The breakthrough data depicted in Figure 3b clearly show that HOF-76a can effectively separate C_2H_6/C_2H_4 mixtures. C_2H_4 gas eluted through the adsorption bed first to yield an outflow of pure gas with an undetectable amount of C_2H_6 (the detection limit of the instrument is 0.01%), affording a desirable purity of over 99.9%. In contrast, C_2H_6 broke through the bed after 27 min because C_2H_6 is more efficiently adsorbed. These experiments are consistent well with simulated breakthrough results. During the breakthrough process of HOF-76a, the pure C_2H_4 production from the outlet effluent for a given cycle was calculated to be 7.2 L/kg (Figure 3b), outperforming most of the top-performing MOFs such as MAF-49 (6.2 L/kg),[12] $Cu(Qc)_2$ (4.4 L/kg),[15] and PCN-250 (3.36 L/kg).[16a] Subsequently, we performed multiple mixed-gas (C_2H_6/C_2H_4 at 50/50) column breakthrough tests to examine the preservation of separation performance of HOF-76a at ambient conditions. The breakthrough times for both C_2H_6 and C_2H_4 remains almost unchanged within six continuous cycles, confirming its good recyclability for C_2H_6/C_2H_4 separation (Figures 3c, S21, and 22).

The feed gases in the practical production of high-purity C_2H_4 sometimes have relatively low C_2H_6 concentrations (6–10%) contaminated by low levels of impurities such as CH_4, H_2, and C_2H_2.[28] We thus conducted a series of breakthrough experiments on HOF-76a for C_2H_6/C_2H_4 (10/90) and $C_2H_6/C_2H_4/CH_4/H_2/C_2H_2$ (10/87/1/1/1) mixtures. As shown in Figures 3d and S23, highly efficient separation was also realized for both gas mixtures, indicating that HOF-76a can be used to purify C_2H_4 from the mixtures with low C_2H_6 concentrations, even in the presence of CH_4, H_2, and C_2H_2 impurities. Additionally, breakthrough experiments under moisture (from 446 to 2130 ppm) revealed that HOF-76a can maintain its separation performance under more extreme moisture conditions than that would be found in a practical process (Figure S24).[29]

Given that an industrial application is potentially under high pressure (typically 5–10 bar),[17a] as required by pressure-swing adsorption (PSA) processes, we thus investigated the separation performance of HOF-76a at 5 bar. The C_2H_6 and C_2H_4 isotherms were measured at 298 K up to 5 bar (Figure S25), wherein the C_2H_6 uptake can increase to 6.3 mmol g^{-1}. Accordingly to IAST calculations for 50/50 and 10/90 mixtures at 5 bar (Figure S26), we found that HOF-76a can maintain its selectivity to around 2. As shown in Figure 3e,f, both the simulated and actual breakthrough curves clearly demonstrated that HOF-76a is capable of removing C_2H_6 from 50/50 and 10/90 C_2H_6/C_2H_4 mixtures at 5 bar and 298 K (Figure S28), and the simulations match well with the experiments (Figure S29). At this high-pressure, the production of high-purity C_2H_4 from the outlet effluent for 50/50 mixtures can be enhanced to 18.8 L/kg, a value comparable to the record $Fe_2(O_2)(dobdc)$[13] (19.3 L/kg at ambient conditions). To the best of our knowledge, this is the first example of porous materials whose reversed C_2H_6/C_2H_4 separation at high pressure has been well established by both simulated and experimental breakthrough, enabling HOF-76a to be a potential material for industrial C_2H_6/C_2H_4 separation application.

CONCLUSION

In summary, we have realized the best example of an ultrarobust HOF adsorbent (HOF-76a) that exhibits the preferential adsorption of ethane over ethylene, affording the unusual reversed C_2H_6/C_2H_4 adsorption. The foregoing results showed that this material not only possesses extraordinary thermal stability and water stability, but also exhibits exceptional C_2H_6/C_2H_4 separation performance superior to most of the C_2H_6-selective MOFs developed. As revealed by DFT calculation results, the nature of nonpolar/inert surfaces in HOF-76a and the suitable triangular channel-like pores to "match" with the C_2H_6 molecule play the important roles for the preferential interactions with C_2H_6 over C_2H_4. Simulated and experimental breakthrough curves confirmed that HOF-76a can efficiently separate C_2H_6 from various C_2H_6/C_2H_4 mixtures to directly produce high-purity C_2H_4 gas at ambient pressure and high pressure conditions, respectively. These results revealed in this work may shed some light on the development of this new kind of HOF materials for the industrially important C_2H_6/C_2H_4 separation in the future.

ASSOCIATED CONTENT

Supporting Information

The Supporting Information is available free of charge at https://pubs.acs.org/doi/10.1021/jacs.9b12428.

Full details for experimental procedures, single crystal X-ray crystallography, gas sorption and stability tests, breakthrough experiments, and DFT calculation data (PDF)

Crystallographic data for HOF-76 (CIF)

AUTHOR INFORMATION

Corresponding Authors

*bin.li@zju.edu.cn
*banglin.chen@utsa.edu

ORCID

Xu Zhang: 0000-0001-9114-1842
Rajamani Krishna: 0000-0002-4784-8530
Hui Wu: 0000-0003-0296-5204
Wei Zhou: 0000-0002-5461-3617
Zhong-Ning Chen: 0000-0003-3589-3745
Bin Li: 0000-0002-7774-5452
Guodong Qian: 0000-0001-7133-2473
Banglin Chen: 0000-0001-8707-8115

Notes

The authors declare no competing financial interest.

DOI: 10.1021/jacs.9b12428
J. Am. Chem. Soc. 2020, 142, 633–640

■ ACKNOWLEDGMENTS

This research was supported by the "Hundred Talent Program" of Zhejiang University and China, the National Science Foundation of China (51803179, 21922810, and 21701171), and Welch Foundation (Grant AX-1730).

■ REFERENCES

(1) Eldridge, R. B. Olefin/paraffin separation technology: a review. *Ind. Eng. Chem. Res.* **1993**, *32* (10), 2208−2212.
(2) Corma, A.; Corresa, E.; Mathieu, Y.; Sauvanaud, L.; Al-Bogami, S.; Al-Ghrami, M. S.; Bourane, A. Crude oil to chemicals: light olefins from crude oil. *Catal. Sci. Technol.* **2017**, *7* (1), 12−46.
(3) (a) Sholl, D. S.; Lively, R. P. Seven chemical separations to change the world. *Nature* **2016**, *532* (7600), 435−437. (b) Chu, S.; Cui, Y.; Liu, N. The path towards sustainable energy. *Nat. Mater.* **2017**, *16*, 16−22.
(4) (a) Furukawa, H.; Cordova, K. E.; O'Keeffe, M.; Yaghi, O. M. The chemistry and applications of metal-organic frameworks. *Science* **2013**, *341* (6149), 974−986. (b) Zhao, X.; Wang, Y.; Li, D. S.; Bu, X.; Feng, P. Metal−organic frameworks for separation. *Adv. Mater.* **2018**, *30* (37), 1705189. (c) Liao, P.-Q.; Huang, N.-Y.; Zhang, W.-X.; Zhang, J.-P.; Chen, X.-M. Controlling guest conformation for efficient purification of butadiene. *Science* **2017**, *356* (6343), 1193−1196. (d) Nugent, P.; Belmabkhout, Y.; Burd, S. D.; Cairns, A. J.; Luebke, R.; Forrest, K.; Pham, T.; Ma, S.; Space, B.; Wojtas, L.; Eddaoudi, M.; Zaworotko, M. J. Porous materials with optimal adsorption thermodynamics and kinetics for CO_2 separation. *Nature* **2013**, *495*, 80−84. (e) Peng, Y.-L.; Pham, T.; Li, P.; Wang, T.; Chen, Y.; Chen, K.-J.; Forrest, K. A.; Space, B.; Cheng, P.; Zaworotko, M. J.; Zhang, Z. Robust ultramicroporous metal-organic frameworks with benchmark affinity for acetylene. *Angew. Chem., Int. Ed.* **2018**, *57* (34), 10971−10975.
(5) Safarik, D. J.; Eldridge, R. B. Olefin/paraffin separations by reactive absorption: a review. *Ind. Eng. Chem. Res.* **1998**, *37* (7), 2571−2581.
(6) (a) Rege, S. U.; Padin, J.; Yang, R. T. Olefin/paraffin separations by adsorption: π-complexation vs. kinetic separation. *AIChE J.* **1998**, *44* (4), 799−809. (b) Aguado, S.; Bergeret, G.; Daniel, C.; Farrusseng, D. Absolute molecular sieve separation of ethylene/ethane mixtures with silver zeolite A. *J. Am. Chem. Soc.* **2012**, *134* (36), 14635−14637. (c) Li, B.; Zhang, Y.; Krishna, R.; Yao, K.; Han, Y.; Wu, Z.; Ma, D.; Shi, Z.; Pham, T.; Space, B.; Liu, J.; Thallapally, P. K.; Liu, J.; Chrzanowski, M.; Ma, S. Introduction of π-complexation into porous aromatic framework for highly selective adsorption of ethylene over ethane. *J. Am. Chem. Soc.* **2014**, *136* (24), 8654−8660. (d) Bereciartua, P. J.; Cantín, Á.; Corma, A.; Jordá, J. L.; Palomino, M.; Rey, F.; Valencia, S.; Corcoran, E. W., Jr.; Kortunov, P.; Ravikovitch, P. I.; Burton, A.; Yoon, C.; Wang, Y.; Paur, C.; Guzman, J.; Bishop, A. R.; Casty, G. L. Control of zeolite framework flexibility and pore topology for separation of ethane and ethylene. *Science* **2017**, *358* (6366), 1068−1071.
(7) (a) Barnett, B. R.; Gonzalez, M. I.; Long, J. R. Recent progress towards light hydrocarbon separations using metal−organic frameworks. *Trends in Chem.* **2019**, *1* (2), 159−171. (b) Wu, H.; Gong, Q.; Olson, D. H.; Li, J. Commensurate adsorption of hydrocarbons and alcohols in microporous metal−organic frameworks. *Chem. Rev.* **2012**, *112* (2), 836−868. (c) Zeng, H.; Xie, M.; Huang, Y.-L.; Zhao, Y.; Xie, X.-J.; Bai, J.-P.; Wan, M.-Y.; Krishna, R.; Lu, W.; Li, D. Induced fit of C_2H_2 in a flexible MOF through cooperative action of open metal sites. *Angew. Chem., Int. Ed.* **2019**, *58* (25), 8515−8519. (d) Cui, W.-G.; Hu, T.-L.; Bu, X.-H. Metal−organic framework materials for the separation and purification of light hydrocarbons. *Adv. Mater.* **2019**, *31* (50), 1806445.
(8) (a) Yang, S.; Ramirez-Cuesta, A. J.; Newby, R.; Garcia-Sakai, V.; Manuel, P.; Callear, S. K.; Campbell, S. I.; Tang, C. C.; Schröder, M. Supramolecular binding and separation of hydrocarbons within a functionalized porous metal−organic framework. *Nat. Chem.* **2015**, *7* (2), 121−129. (b) Bloch, E. D.; Queen, W. L.; Krishna, R.; Zadrozny, J. M.; Brown, C. M.; Long, J. R. Hydrocarbon separations in a metal−organic framework with open iron(II) coordination sites. *Science* **2012**, *335* (6076), 1606−1610. (c) Wang, H.; Dong, X.; Colombo, V.; Wang, Q.; Liu, Y.; Liu, W.; Wang, X.-L.; Huang, X.-Y.; Proserpio, D. M.; Sironi, A.; Han, Y.; Li, J. Tailor-made microporous metal−organic frameworks for the full separation of propane from propylene through selective size exclusion. *Adv. Mater.* **2018**, *30* (49), 1805088. (d) Cadiau, A.; Adil, K.; Bhatt, P. M.; Belmabkhout, Y.; Eddaoudi, M. A metal-organic framework−based splitter for separating propylene from propane. *Science* **2016**, *353* (6295), 137−140.
(9) Li, J.-R.; Kuppler, R. J.; Zhou, H.-C. Selective gas adsorption and separation in metal−organic frameworks. *Chem. Soc. Rev.* **2009**, *38* (5), 1477−1504.
(10) Yang, R. T. *Adsorbents: Fundamentals and Applications*; John Wiley & Sons, Inc.: Hoboken, NJ, 2003.
(11) (a) Rowsell, J. L. C.; Spencer, E. C.; Eckert, J.; Howard, J. A. K.; Yaghi, O. M. Gas adsorption sites in a large-pore metal-organic framework. *Science* **2005**, *309* (5739), 1350−1354. (b) Bae, Y.-S.; Lee, C. Y.; Kim, K. C.; Farha, O. K.; Nickias, P.; Hupp, J. T.; Nguyen, S. T.; Snurr, R. Q. High propene/propane selectivity in isostructural metal-organic frameworks with high densities of open metal sites. *Angew. Chem., Int. Ed.* **2012**, *51* (8), 1857−1860.
(12) Liao, P.-Q.; Zhang, W.-X.; Zhang, J.-P.; Chen, X.-M. Efficient purification of ethene by an ethane-trapping metal-organic framework. *Nat. Commun.* **2015**, *6*, 8697.
(13) Li, L.; Lin, R.-B.; Krishna, R.; Li, H.; Xiang, S.; Wu, H.; Li, J.; Zhou, W.; Chen, B. Ethane/ethylene separation in a metal-organic framework with iron-peroxo sites. *Science* **2018**, *362* (6413), 443−446.
(14) Qazvini, O. T.; Babarao, R.; Shi, Z.-L.; Zhang, Y.-B.; Telfer, S. G. A robust ethane-trapping metal−organic framework with a high capacity for ethylene purification. *J. Am. Chem. Soc.* **2019**, *141* (12), 5014−5020.
(15) Lin, R.-B.; Wu, H.; Li, L.; Tang, X.-L.; Li, Z.; Gao, J.; Cui, H.; Zhou, W.; Chen, B. Boosting ethane/ethylene separation within isoreticular ultramicroporous metal-organic frameworks. *J. Am. Chem. Soc.* **2018**, *140* (40), 12940−12946.
(16) (a) Chen, Y.; Qiao, Z.; Wu, H.; Lv, D.; Shi, R.; Xia, Q.; Zhou, J.; Li, Z. An ethane-trapping MOF PCN-250 for highly selective adsorption of ethane over ethylene. *Chem. Eng. Sci.* **2018**, *175*, 110−117. (b) Lv, D.; Shi, R.; Chen, Y.; Wu, Y.; Wu, H.; Xi, H.; Xia, Q.; Li, Z. Selective adsorption of ethane over ethylene in PCN-245: impacts of interpenetrated adsorbent. *ACS Appl. Mater. Interfaces* **2018**, *10* (9), 8366−8373. (c) Hartmann, M.; Böhme, U.; Hovestadt, M.; Paula, C. Adsorptive separation of olefin/paraffin mixtures with ZIF-4. *Langmuir* **2015**, *31* (45), 12382−12389. (d) Böhme, U.; Barth, B.; Paula, C.; Kuhnt, A.; Schwieger, W.; Mundstock, A.; Caro, J.; Hartmann, M. Ethene/ethane and propene/propane separation via the olefin and paraffin selective metal−organic framework adsorbents CPO-27 and ZIF-8. *Langmuir* **2013**, *29* (27), 8592−8600. (e) Zeng, H. Cage-interconnected metal−organic framework with tailored apertures for efficient C2H6/C2H4 separation under humid conditions. *J. Am. Chem. Soc.* **2019**, DOI: 10.1021/jacs.9b10923.
(17) (a) Pires, J.; Fernandes, J.; Dedecker, K.; Gomes, J. R. B.; Pérez-Sánchez, G.; Nouar, F.; Serre, C.; Pinto, M. L. Enhancement of ethane selectivity in ethane-ethylene mixtures by perfluoro groups in Zr-based metal-organic frameworks. *ACS Appl. Mater. Interfaces* **2019**, *11* (30), 27410−27421. (b) Pires, J.; Pinto, M. L.; Saini, V. Ethane selective IRMOF-8 and its significance in ethane-ethylene separation by adsorption. *ACS Appl. Mater. Interfaces* **2014**, *6* (15), 12093−12099. (c) Gücüyener, C.; van den Bergh, J.; Gascon, J.; Kapteijn, F. Ethane/ethene separation turned on its head: selective ethane adsorption on the metal-organic framework ZIF-7 through a gate-opening mechanism. *J. Am. Chem. Soc.* **2010**, *132* (50), 17704−17706. (d) Pillai, R. S.; Pinto, M. L.; Pires, J.; Jorge, M.; Gomes, J. R. B. Understanding gas adsorption selectivity in IRMOF-8 using molecular simulation. *ACS Appl. Mater. Interfaces* **2015**, *7* (1), 624−637. (e) Lahoz-Martín, F. D.; Martin-Calvo, A.; Gutierrez-Sevillano, J. J.; Calero, S. Effect of light gases in the ethane/ethylene separation using

DOI: 10.1021/jacs.9b12428
J. Am. Chem. Soc. 2020, 142, 633−640

zeolitic imidazolate frameworks. *J. Phys. Chem. C* **2018**, *122* (15), 8637−8646. (f) Ribeiro, R. P. P. L.; Camacho, B. C. R.; Lyubchyk, A.; Esteves, I. A. A. C.; Cruz, F. J. A. L.; Mota, J. P. B. Experimental and computational study of ethane and ethylene adsorption in the MIL-53(Al) metal-organic framework. *Microporous Mesoporous Mater.* **2016**, *230*, 154−165.

(18) (a) Lin, R.-B.; He, Y.; Li, P.; Wang, H.; Zhou, W.; Chen, B. Multifunctional porous hydrogen-bonded organic framework materials. *Chem. Soc. Rev.* **2019**, *48* (5), 1362−1389. (b) Hisaki, I.; Xin, C.; Takahashi, K.; Nakamura, T. Designing hydrogen-bonded organic frameworks (HOFs) with permanent porosity. *Angew. Chem., Int. Ed.* **2019**, *58* (33), 11160−11170. (c) Yang, W.; Greenaway, A.; Lin, X.; Matsuda, R.; Blake, A. J.; Wilson, C.; Lewis, W.; Hubberstey, P.; Kitagawa, S.; Champness, N. R.; Schröder, M. Exceptional thermal stability in a supramolecular organic framework: porosity and gas storage. *J. Am. Chem. Soc.* **2010**, *132* (41), 14457−14469.

(19) (a) Venkataraman, D.; Lee, S.; Zhang, J.; Moore, J. S. An organic solid with wide channels based on hydrogen bonding between macrocycles. *Nature* **1994**, *371* (6498), 591−593. (b) Maly, K. E.; Gagnon, E.; Maris, T.; Wuest, J. D. Engineering hydrogen-bonded molecular crystals built from derivatives of hexaphenylbenzene and related compounds. *J. Am. Chem. Soc.* **2007**, *129* (14), 4306−4322. (c) He, Y.; Xiang, S.; Chen, B. A microporous hydrogen-bonded organic framework for highly selective C_2H_2/C_2H_4 separation at ambient temperature. *J. Am. Chem. Soc.* **2011**, *133* (37), 14570−14573.

(20) (a) Han, B.; Wang, H.; Wang, C.; Wu, H.; Zhou, W.; Chen, B.; Jiang, J. Postsynthetic metalation of a robust hydrogen-bonded organic framework for heterogeneous catalysis. *J. Am. Chem. Soc.* **2019**, *141* (22), 8737−8740. (b) Luo, X.-Z.; Jia, X.-J.; Deng, J.-H.; Zhong, J.-L.; Liu, H.-J.; Wang, K.-J.; Zhong, D.-C. A microporous hydrogen-bonded organic framework: exceptional stability and highly selective adsorption of gas and liquid. *J. Am. Chem. Soc.* **2013**, *135* (32), 11684−11687. (c) Chen, T.-H.; Popov, I.; Kaveevivitchai, W.; Chuang, Y.-C.; Chen, Y.-S.; Daugulis, O.; Jacobson, A. J.; Miljanić, O. Š. Thermally robust and porous noncovalent organic framework with high affinity for fluorocarbons and CFCs. *Nat. Commun.* **2014**, *5*, 5131. (d) Yoon, T.-U.; Baek, S. B.; Kim, D.; Kim, E.-J.; Lee, W.-G.; Singh, B. K.; Lah, M. S.; Bae, Y.-S.; Kim, K. S. Efficient separation of C_2 hydrocarbons in a permanently porous hydrogen-bonded organic framework. *Chem. Commun.* **2018**, *54* (67), 9360−9363.

(21) (a) Mastalerz, M.; Oppel, I. M. Rational construction of an extrinsic porous molecular crystal with an extraordinary high specific surface area. *Angew. Chem., Int. Ed.* **2012**, *51* (21), 5252−5255. (b) Pulido, A.; Chen, L.; Kaczorowski, T.; Holden, D.; Little, M. A.; Chong, S. Y.; Slater, B. J.; McMahon, D. P.; Bonillo, B.; Stackhouse, C. J.; Stephenson, A.; Kane, C.; Clowes, M. R.; Hasell, T.; Cooper, A. I.; Day, G. M. Functional materials discovery using energy−structure−function maps. *Nature* **2017**, *543* (7647), 657−664. (c) Bao, Z.; Xie, D.; Chang, G.; Wu, H.; Li, L.; Zhou, W.; Wang, H.; Zhang, Z.; Xing, H.; Yang, Q.; Zaworotko, M. J.; Ren, Q.; Chen, B. Fine tuning and specific binding sites with a porous hydrogen-bonded metal-complex framework for gas selective separations. *J. Am. Chem. Soc.* **2018**, *140* (13), 4596−4603.

(22) (a) Hisaki, I.; Nakagawa, S.; Tohnai, N.; Miyata, M. A C_3-symmetric macrocycle-based, hydrogen-bonded, multiporous hexagonal network as a motif of porous molecular crystals. *Angew. Chem., Int. Ed.* **2015**, *54* (10), 3008−3012. (b) Hu, F.; Liu, C.; Wu, M.; Pang, J.; Jiang, F.; Yuan, D.; Hong, M. An ultrastable and easily regenerated hydrogen-bonded organic molecular framework with permanent porosity. *Angew. Chem., Int. Ed.* **2017**, *56* (8), 2101−2104. (c) Yin, Q.; Zhao, P.; Sa, R.-J.; Chen, G.-C.; Lg, J.; Liu, T.-F.; Cao, R. An ultra-robust and crystalline redeemable hydrogen-bonded organic framework for synergistic chemo-photodynamic therapy. *Angew. Chem., Int. Ed.* **2018**, *57* (26), 7691−7696. (d) Li, P.; Li, P.; Ryder, M. R.; Liu, Z.; Stern, C. L.; Farha, O. K.; Stoddart, J. F. Interpenetration isomerism in triptycene-based hydrogen-bonded organic frameworks. *Angew. Chem., Int. Ed.* **2019**, *58* (6), 1664−1669.

(23) Kobayashi, K.; Kobayashi, N. Synthesis and self-Association, absorption, and fluorescence properties of differentially functionalized hexakis(p-substituted-phenylethynyl)benzenes. *J. Org. Chem.* **2004**, *69*, 2487−2497.

(24) Sheldrick, G. M. *SHELXL-97, Program for the refinement of crystal structures*; University of Göttingen: Göttingen, Germany, 1997.

(25) Spek, A. L. Single-crystal structure validation with the program PLATON. *J. Appl. Crystallogr.* **2003**, *36*, 7−13.

(26) Giannozzi, P.; Baroni, S.; Bonini, N.; Calandra, M.; Car, R.; Cavazzoni, C.; Ceresoli, D.; Chiarotti, G. L.; Cococcioni, M.; Dabo, I.; Dal Corso, A.; Fabris, S.; Fratesi, G.; de Gironcoli, S.; Gebauer, R.; Gerstmann, U.; Gougoussis, C.; Kokalj, A.; Lazzeri, M.; Martin-Samos, L.; Marzari, N.; Mauri, F.; Mazzarello, R.; Paolini, S.; Pasquarello, A.; Paulatto, L.; Sbraccia, C.; Scandolo, S.; Sclauzero, G.; Seitsonen, A. P.; Smogunov, A.; Umari, P.; Wentzcovitch, R. M. QUANTUM ESPRESSO: a modular and open-source software project for quantum simulations of materials. *J. Phys.: Condens. Matter* **2009**, *21* (39), 395502.

(27) Barone, V.; Casarin, M.; Forrer, D.; Pavone, M.; Sambi, M.; Vittadini, A. J. Role and effective treatment of dispersive forces in materials: Polyethylene and graphite crystals as test cases. *J. Comput. Chem.* **2009**, *30* (6), 934−939.

(28) Meyers, R. A. *Handbook of Petrochemicals Production Processes*; McGraw-Hill: New York, 2005.

(29) (a) Sundaram, K. M.; Shreehan, M. M.; Olszewski, E. F. Ethylene. *Firk-Othmer Encyclopedia of Chemical Technology*; Wiley Online Library: New York, 2001. (b) Cui, X.; Chen, K.; Xing, H.; Yang, Q.; Krishna, R.; Bao, Z.; Wu, H.; Zhou, W.; Dong, X.; Han, Y.; Li, B.; Ren, Q.; Zaworotko, M. J.; Chen, B. Pore chemistry and size control in hybrid porous materials for acetylene capture from ethylene. *Science* **2016**, *353* (6295), 141−144. (c) Lin, R.-B.; Li, L.; Zhou, H.-L.; Wu, H.; He, C.; Li, S.; Krishna, R.; Li, J.; Zhou, W.; Chen, B. Molecular sieving of ethylene from ethane using a rigid metal−organic framework. *Nat. Mater.* **2018**, *17*, 1128−1133.

DOI: 10.1021/jacs.9b12428
J. Am. Chem. Soc. 2020, 142, 633−640

Supplementary Information

Selective Ethane/Ethylene Separation in a Robust Microporous Hydrogen-Bonded Organic Framework

Xu Zhang,[†,‡] Libo Li,[§,∥] Jia-Xin Wang,[†] Hui-Min Wen,[⊥] Rajamani Krishna,[#] Hui Wu,[▽] Wei Zhou,[▽] Zhong-Ning Chen,[‡] Bin Li,[†] Guodong Qian,[†] and Banglin Chen*[,∥]*

[†] State Key Laboratory of Silicon Materials, School of Materials Science and Engineering, Zhejiang University, Hangzhou 310027, China

[‡] State Key Laboratory of Structural Chemistry, Fujian Institute of Research on the Structure of Matter, Chinese Academy of Sciences, Fuzhou, Fujian 350002, China.

[§] College of Chemistry and Chemical Engineering, Taiyuan University of Technology, Taiyuan 030024, Shanxi, P. R. China

[∥] Department of Chemistry, University of Texas at San Antonio, One UTSA Circle, San Antonio, TX 78249-0698, United States

[⊥] College of Chemical Engineering, Zhejiang University of Technology, Zhejiang, 310014, P. R. China

[#] Van 't Hoff Institute for Molecular Sciences, University of Amsterdam, Science Park 904, 1098 XH Amsterdam, The Netherlands

[▽] NIST Center for Neutron Research, National Institute of Standards and Technology, Gaithersburg, MD 20899-6102, United States

1. General materials and procedures

All starting chemicals and solvents were purchased from commercial companies and used without further purification: hexabromobenzene (Alfa Aesar, 97%); ethyl 4-ethynylbenzoate was prepared from 4-Bromobenzoic acid (Alfa Aesar, 98+%); $Pd(PPh_3)_2Cl_2$ (Aladdin, 98+%); CuI (Acros, 98%); PPh_3 (Greagent, 99+%); trimethylsilylacetylene (Macklin, 98+%); D_2O (Sigma-Alderich, 99.9 atom%); NaOD (Norell, 30 WT% in D_2O, 99.9 atom%); DCl (Sigma-Alderich, 35 WT% in D_2O, 99+ atom%). ^1H and ^{13}C NMR spectra were recorded on Bruker AVANCE III spectrometers (400 MHz). Thermogravimetric analyses (TGA) were performed on a Netzsch STA 449C thermal analyzer from 30 to 800 °C under nitrogen atmosphere at a heating rate of 5 °C/minute rate. Powder X–ray diffraction (PXRD) patterns were measured by a BRUKER D8 ADVANCE diffractometer employing Cu-K_α radiation operated at 30 kV and 15 mA, scanning over the range 2-45° (2θ) at a rate of 2°/min.

C_2H_4 (99.99%), C_2H_6 (99.99%), He (99.999%) and mixed gases of C_2H_4/C_2H_6 = 10/90 (v/v), C_2H_4/C_2H_6 = 50/50 (v/v), and $C_2H_6/C_2H_4/C_2H_2/CH_4/H_2$ (10/87/1/1/1) mixtures were purchased from Beijing Special Gas Co. LTD (China).

2. Fitting of pure component isotherms

The pure component isotherm data for C_2H_4 and C_2H_6 in HOF-76 were measured at 273 K and 296 K. The data were fitted with the 1-site Langmuir-Freundlich model

$$q = q_{sat}\frac{bp^{\nu}}{1+bp^{\nu}}$$

The parameter b is temperature dependent

$$b = b_0 \exp\left(E/RT\right)$$

The fitted parameter values are provided in Table S1-S2 and Figure S27.

3. Isosteric heat of adsorption

The binding energy is reflected in the isosteric heat of adsorption, Q_{st}, defined as

$$Q_{st} = RT^2 \left(\frac{\partial \ln p}{\partial T} \right)_q$$

The Q_{st} values as function of the molar loadings are provided in Figure S16.

4. IAST calculations of adsorption selectivities

The selectivity of preferential adsorption of component 1 (C_2H_6) over component 2 (C_2H_4) can be defined as

$$S_{ads} = \frac{q_1/q_2}{p_1/p_2}$$

Where q_1 and q_2 are the *absolute* component loadings of the adsorbed phase in the mixture, and p_1 and p_2 are the component partial pressures. The component loadings and adsorption selectivity S_{ads} for 50/50 C_2H_6(1)/C_2H_4(2) and 10/90 C_2H_6(1)/C_2H_4(2) mixtures in HOF-76a at 296 K were determined using IAST.

5. Breakthrough simulations

The performance of industrial fixed bed adsorbers is dictated by a combination of adsorption selectivity and uptake capacity. Transient breakthrough simulations were carried out for 50/50 C_2H_6(1)/C_2H_4(2) and 10/90 C_2H_6(1)/C_2H_4(2) mixtures in HOF-76 operating at 298 K and a total pressure of 1 bar or 5 bar respectively, using the methodology described in earlier publications.[1,2] For the breakthrough simulations, the following parameter values were used: length of packed bed, L = 0.3 m; voidage of packed bed, ε = 0.4; superficial gas velocity at inlet, u = 0.04 m/s. The transient breakthrough simulation results are presented in terms of a *dimensionless* time, $\tau = \frac{tu}{L\varepsilon}$, defined by dividing the actual time, t, by the characteristic time, $\frac{L\varepsilon}{u}$.

The breakthrough simulations demonstrate the potential of producing product gas C_2H_4 of required purity during the interval $\Delta\tau$.

6. Stability studies

To investigate the chemical stabilities of HOF-76, the as-synthesized samples were soaked in water, HCl (pH = 1) and NaOH (pH = 10) solutions for 24 hours, respectively. After that, each sample was filtered and washed with water and acetone quickly, and then characterized by PXRD measurements in order to determine whether the sample retains its structural integrity. Subsequently, each sample was solvent-exchanged with dry acetone at least 8 times within two days to completely remove the hardly volatile H_2O molecules in the pores, and then was activated by the activation conditions prior to gas sorption measurements. The 77 K N_2 and 296 K C_2H_6 sorption isotherms were examined to further determine the chemical stability of HOF-76. The thermal stability of HOF-76 was studied by thermogravimetric analysis and various temperature PXRD patterns. The sample for temperature PXRD patterns was treated with 100°, 150°, 200°, 300° for 2 hours, respectively, and then characterized by PXRD measurements. To further check the thermal stability, the sample treated with 300° was solvent-exchanged by dry acetone and then activated to examine the 77 K N_2 and 296 K C_2H_6 sorption isotherms.

To further confirm its ultrahigh chemical stability in acid and base solutions, the samples were also soaked into pH = 10 NaOD solution (0.01 mol/L NaOD in D_2O solution) and pH = 1 HCl solution (0.1 mol/L DCl in D_2O solution), respectively. After 24 hours, the D_2O solution was directly used to measure ^1H NMR spectra. As shown in Figure S11, there is no any signal of HCEB ligand observed, strongly demonstrating that the HOF-76 framework remains stable in these acid and base solutions and no ligands are dissociated into the D_2O solution.

Considering that the C_2H_4 feed gas in industry is often contaminated by trace levels of H_2O (5-50 ppm), the effect of moisture on breakthrough experiments was carried out on HOF-76a for 50/50 C_2H_6/C_2H_4 mixtures containing trace H_2O (from 446 to 2130 ppm) that are more extreme than that found in a realistic process. Figure S24 showed that the presence of trace H_2O has a negligible effect on the breakthrough performance of HOF-76a.

Notation

b	Langmuir-Freundlich constant, $Pa^{-\nu}$
q	component molar loading of species i, mol kg^{-1}
q_{sat}	saturation loading, mol kg^{-1}
L	length of packed bed adsorber, m
t	time, s
T	absolute temperature, K
u	superficial gas velocity in packed bed, m s^{-1}

Greek letters

ε	voidage of packed bed, dimensionless
ν	Freundlich exponent, dimensionless
τ	time, dimensionless

Table S1. 1-site Langmuir-Freundlich parameter fits for C_2H_4 and C_2H_6 in HOF-76 at 1 bar and room temperature.

	q_{sat} mol kg^{-1}	b_0 Pa$^{-\nu}$	E kJ mol^{-1}	ν dimensionless
C_2H_4	6.3	5.25E-13	35	1.14
C_2H_6	5	2.53E-12	31	1.25

Table S2. 1-site Langmuir-Freundlich parameter fits for C_2H_4 and C_2H_6 in HOF-76 at 5 bar and 298 K.

	q_{sat} mol kg^{-1}	b Pa^{-1}	R^2
C_2H_4	11.9	1.73674E-06	0.9953
C_2H_6	9	4.846E-06	0.9857

Table S3. Crystallographic data and structure refinement results of HOF-76.

	HOF-76
Formula	$C_{60}H_{30}O_{12}$
Formula weight	942.84
Temperature/K	100(2)
Crystal system	Monoclinic
Space group	*C*2/c
a, *b* (Å)	22.539(3), 40.639(5)
c (Å)	13.7223(17)
α (°)	90.00
β (°)	96.088(5)
γ (°)	90.00
V (Å^3)	12498(3)
Z	8
D_{calcd} (g cm^{-3})	1.002
μ (mm^{-1})	0.070
F(000)	3888.0
Crystal size/mm^3	0.0032 × 0.0028 × 0.0028
GOF	1.005
R_{int}	0.1562
R_1, wR_2 [I>=2σ (I)]	0.0772, 0.2123
R_1, wR_2 [all data]	0.1799, 0.2684
CCDC number	1907797

[a] $R1 = \Sigma|F_o - F_c|/\Sigma F_o$, [b] $wR2 = \Sigma[w(F_o^2 - F_c^2)^2]/\Sigma[w(F_o)^2)]^{1/2}$

Table S4. Comparison of the density and features of H-bonds, the distance of π···π interactions, and the surface area in HOF-76 and some selected carboxylic acid-type HOFs with established porosities.

carboxylic acid-type HOFs	Number of carboxylic acids	Density of H-bonds (mmol/cm^3)	$d_{O\text{-}H\cdots O}$ (Å)[a]	Angel of O-H···O bonds[b]	$d_{\pi\cdots\pi\ stacking}$ (Å)[c]	S_{BET} ($m^2\ g^{-1}$)[d]	Ref.
HOF-76	**6**	**6.276**	**2.622**	**171.2**	**3.352**	**1121**	**This work**
HOF-TCBP	4	4.355	2.620	176.3	3.425	2066	[3]
PFC-1	4	4.342	2.597	176.0	3.338	2122	[4]
Ex-1	6	3.120	2.551-2.697	170.4	3.446	–	[5]
T12-1	6	5.765	2.565-2.816	173.8	3.459	557	[5]
PETHOF-1a	6	0.994	2.580	161.8	–	1140	[6]
PETHOF-2a	6	2.553	2.600	160.6	3.30	1690	[6]
HOF-BTB	3	3.254	2.594	166.4	–	955	[7]
IISERP-HOF1	3	4.067	2.592	165.2	–	1025	[8]
TCF-1	4	4.995	2.823	152.6	3.600	–	[9]

[a] The distance of O–H···O; [b] the O–H···O bond angel; [c] the distance of π···π stacking interaction; [d] BET surface areas calculated from 77 K N_2 or 195 K CO_2 isotherms.

Table S5. Summary of separation metrics of top-performing ethane-selective materials reported in the literature at 1 bar and room temperature (RT).

C_2H_6-selective adsorbents	C_2H_6 uptake[a] (mmol/g)	C_2H_4 uptake[a] (mmol/g)	Uptake ratio[b] (%)	Selectivity[c]	$Q_{st,\ ethane}$ (kJ/mol)[d]	Productivity$_{exp}$ (L/kg)[e]	Ref.
HOF-76a	**2.95**	**1.67**	**177**	**2.05**	**22.8**	**7.2/18.8[f]**	**This work**
Fe_2O_2(dobdc)	3.32	2.53	131	4.4	66.8	19.3	[10]
MUF-15	4.69[c]	4.15[c]	113[c]	1.94[c]	29.2	14	[11]
MAF-49	1.73	1.69	102	2.7	61	6.2	[12]
$Cu(Qc)_2$	1.85	0.78	235	3.4	29	4.4	[13]
UiO-66-2CF_3	0.86	0.50	171	2.5	30	-	[14]
PCN-250	5.20	4.22	123	1.9	23.2	3.36	[15]
UiO-66	2.38	1.72	138	1.8	-	-	[14]
UiO-66-NDC	4.3	3.46	124	1.4	-	-	[14]
PCN-245	3.27	2.39	137	1.9	22.8	5.8	[16]
$[Ni(bdc)(ted)_{0.5}$	5.0	3.4	147	1.6	21.5	-	[17]
MIL-53(Al)	2.16[g]	1.72[g]	126	1.6	22.5	-	[18]
MIL-142(A)	3.8	2.9	131	1.5	-	-	[14]
IR-MOF-8	4.3	3.0	143	1.8	52.5	2.5	[19]
ZIF-8[h]	2.52	1.51	167	1.7	17.2	0.4	[20]
ZIF-7	1.83	1.80	102	1.5	-	2	[21]
ZIF-4[h]	2.30	2.20	104	2.15	-	6.6	[22]
UTSA-35	2.43	2.16	112	1.4	-	-	[10]
HOF-BTB[i]	3.09	2.48	124	1.4	25.4	-	[23]

[a] At 1 bar and room temperature; [b] C_2H_6/C_2H_4 uptake ratio at 1 bar and RT; [c] IAST selectivity for 50/50 C_2H_6/C_2H_4 gas mixtures; [d] The adsorption heat (Q_{st}) of C_2H_6 at low surface coverage. [e] The pure C_2H_4 productivity calculated from breakthrough experiments at 1 bar and RT on 50/50 gas mixtures. [f] The pure C_2H_4 productivity under 5.0 bar and RT. [g] At 323 K. [h] At 293K. [i] The reported literature only described the C_2H_4 and C_2H_6 adsorption isotherms, so the selectivity and uptake ratio were evaluated based on these isotherms.

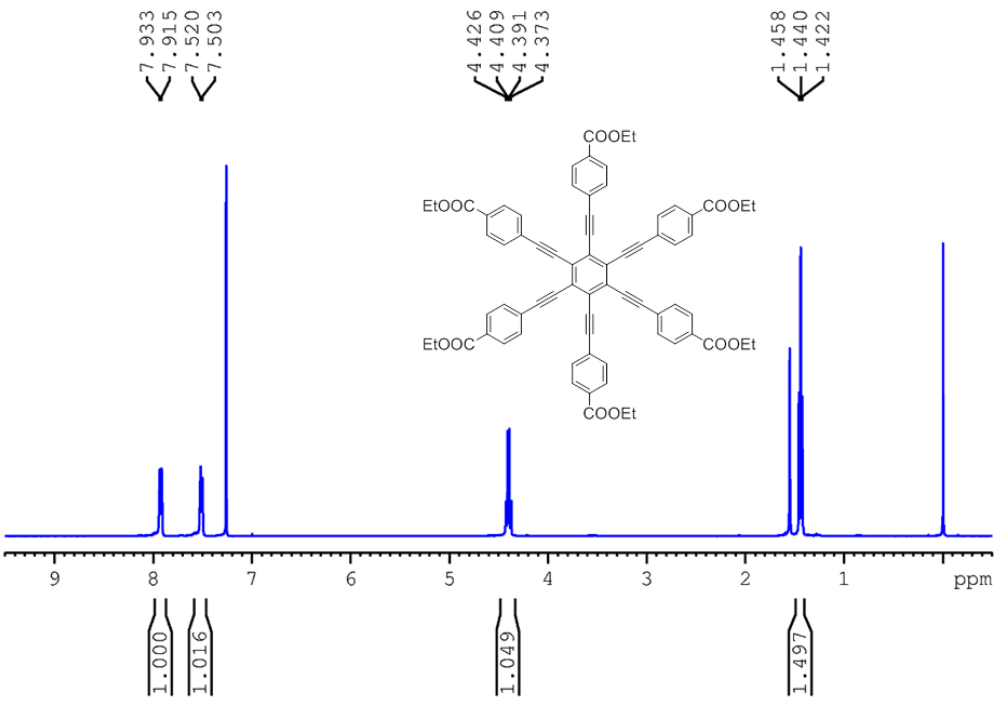

Figure S1. ^{1}H NMR ($CDCl_3$, 400 MHz) spectrum of compound **1**.

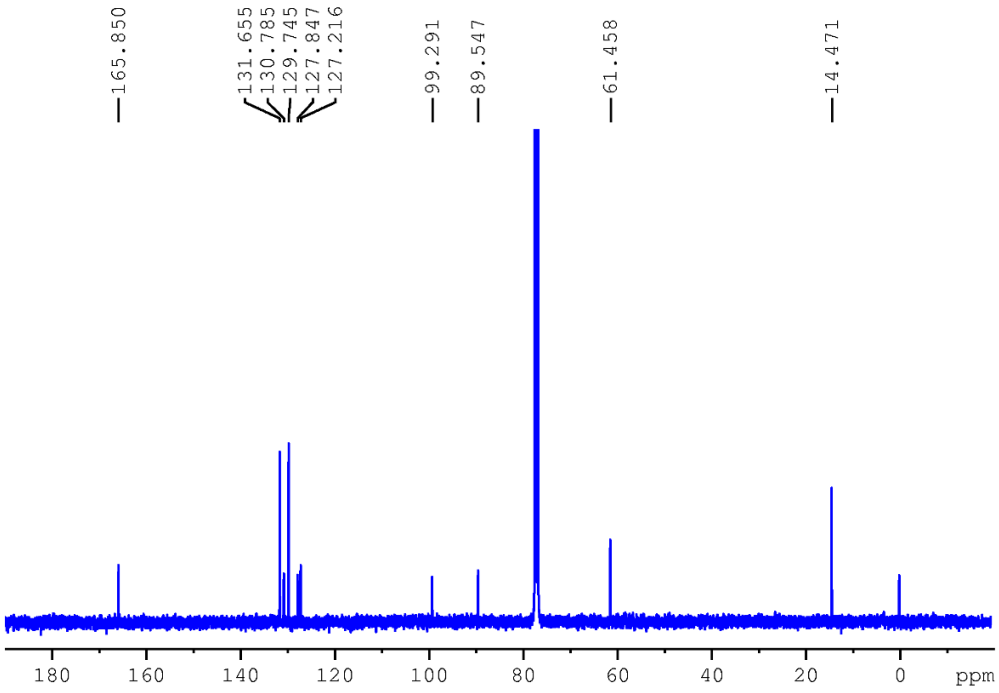

Figure S2. ^{13}C NMR ($CDCl_3$, 100 MHz) spectrum of compound **1**.

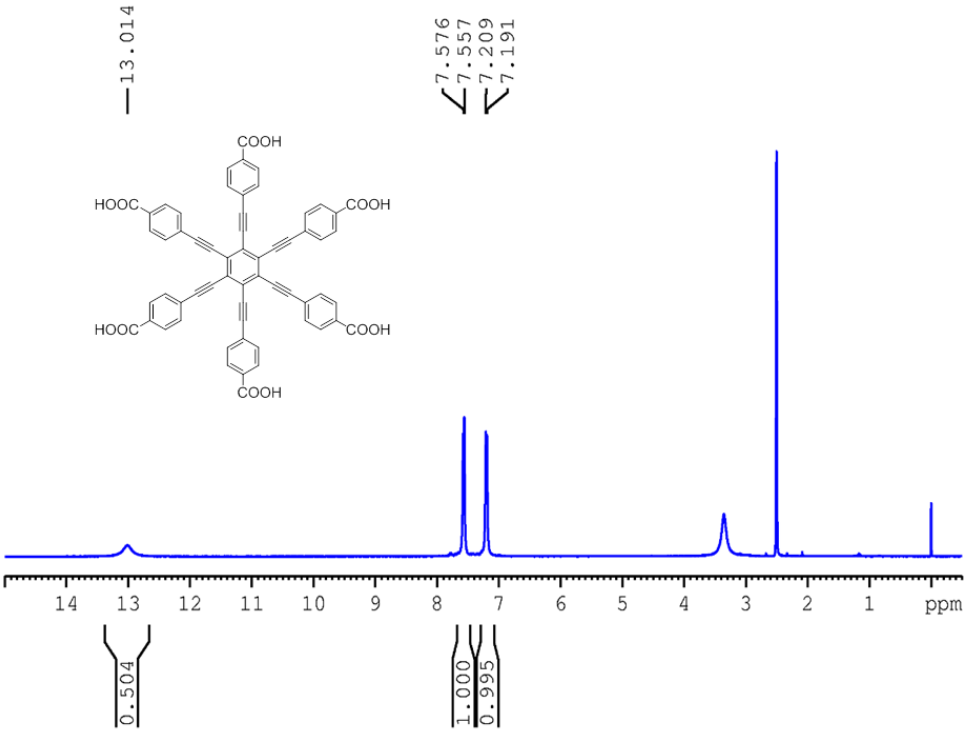

Figure S3. ^{1}H NMR (DMSO-d_6, 400 MHz) spectrum of compound **HCEB**.

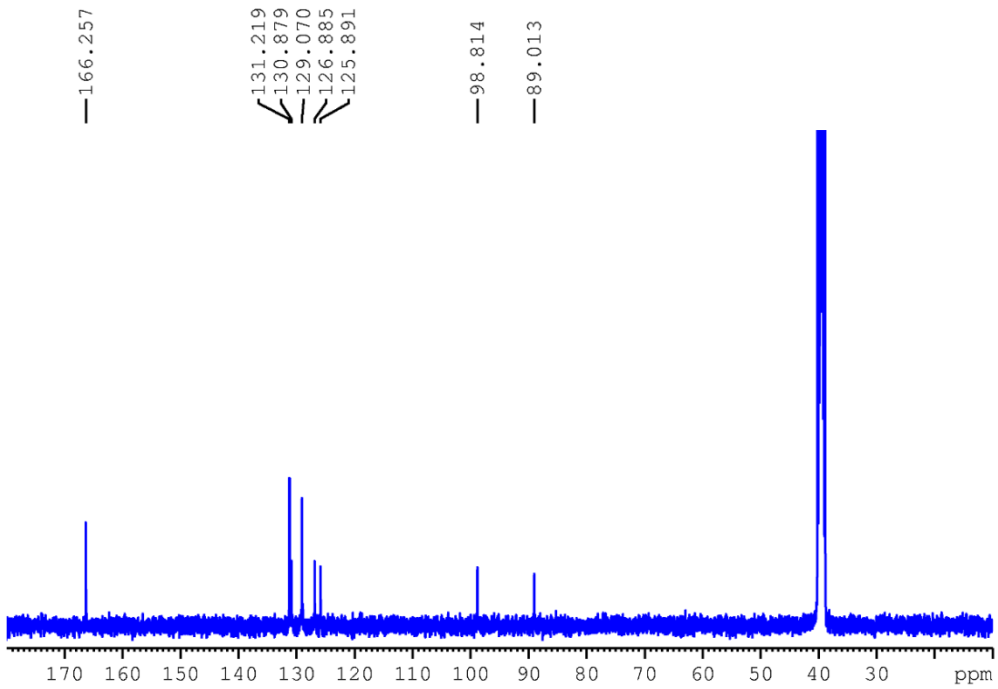

Figure S4. ^{13}C NMR (DMSO-d_6, 100 MHz) spectrum of compound **HCEB**.

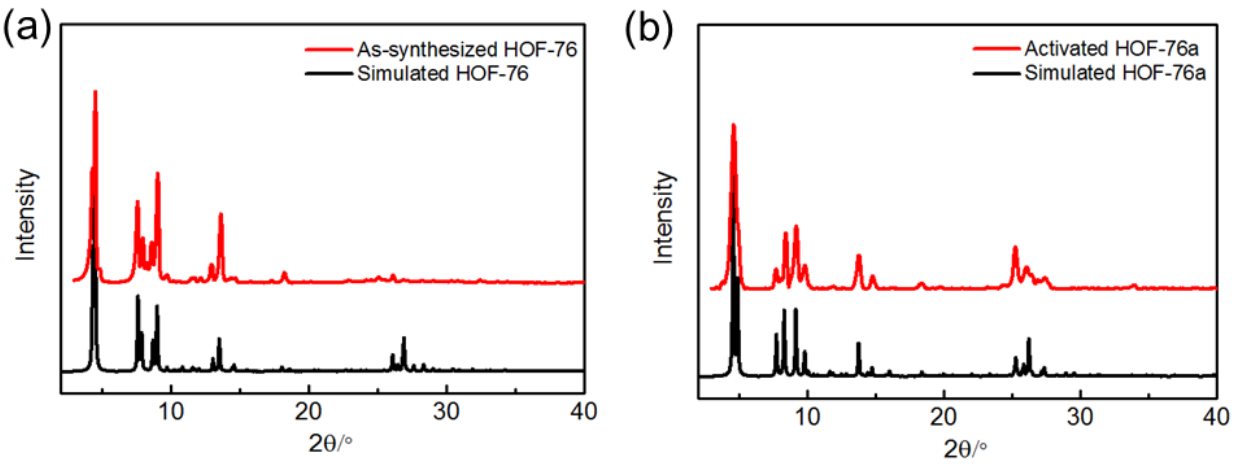

Figure S5. (a) Experimental PXRD pattern of as-synthesized HOF-76 (red) and the calculated pattern based on the single-crystal X-ray structure (black). (b) Experimental PXRD pattern of activated HOF-76a (red) and the calculated pattern based on the HOF-76a structural model (black). The agreement between experiment and simulation is very well. In the HOF-76a structural model, the lattice parameters were obtained from indexing the experimental PXRD pattern of activated HOF-76a. The results show that the HOF-76 crystal structure remains essentially the same upon activation (guest removal), in terms of crystal symmetry and framework arrangement. However, the unit cell parameters do change a bit: As-synthesized HOF-76 (from SXRD data): *a*=22.539; *b*=40.639; *c*=13.722; beta=96.088; Activated HOF-76 (from PXRD data): *a*=23.051; *b*=36.025; *c*=14.229; beta=98.095.

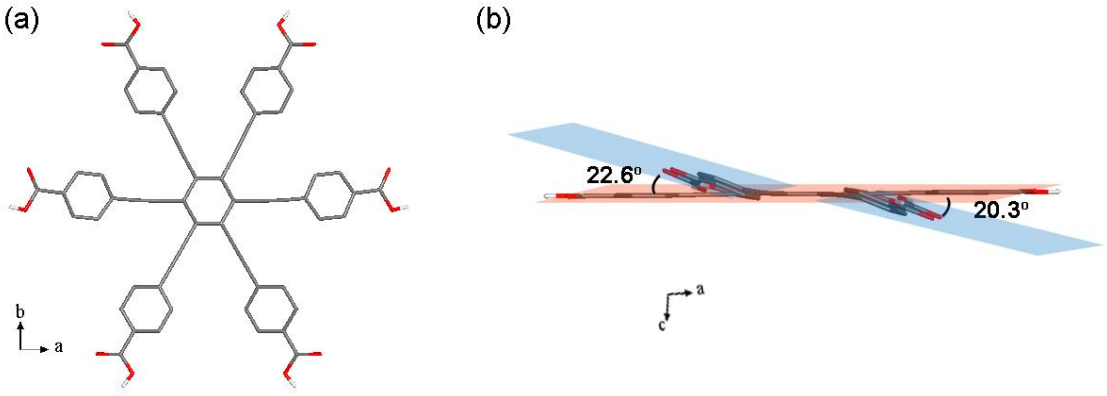

Figure S6. (a) View of the HCEB ligand along *c*-axis; (b) along *b*-axis, indicating that the four outer carboxyphenyl groups alternately direct up and down against the plane of the central benzene ring.

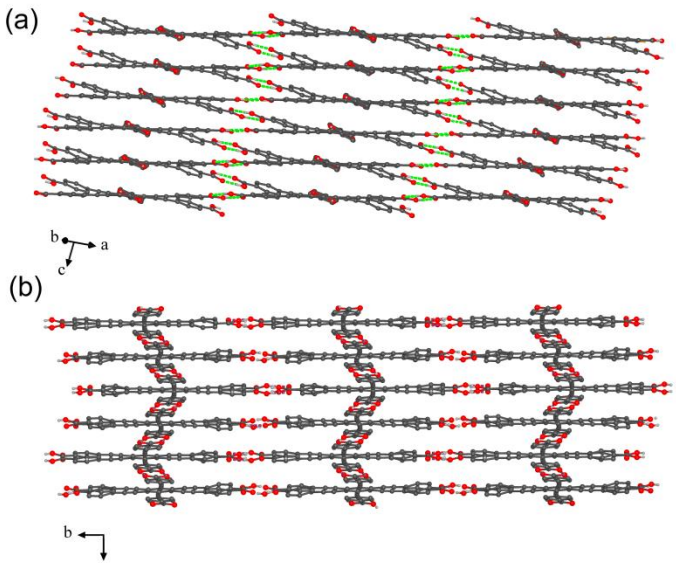

Figure S7. Crystal structure description of HOF-76, showing the hydrogen-bonding connections of the HCEB building blocks to form a three-dimensionally extended H-bonded network viewed two perpendicular directions to channels.

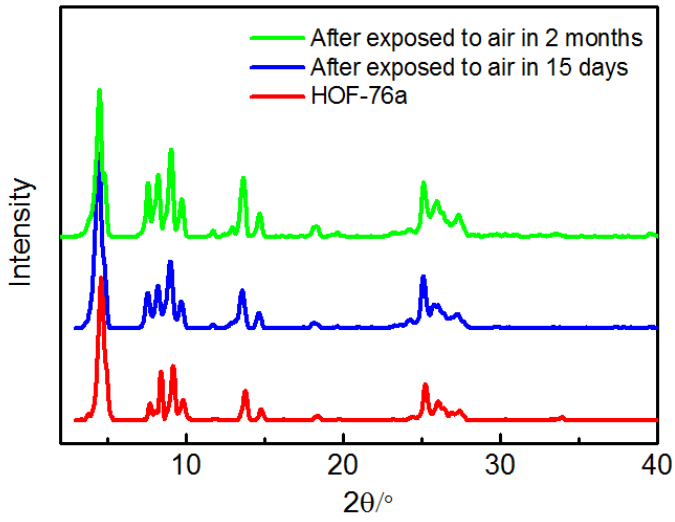

Figure S8. PXRD patterns of activated HOF-76a samples after exposed to air for more than 2 months.

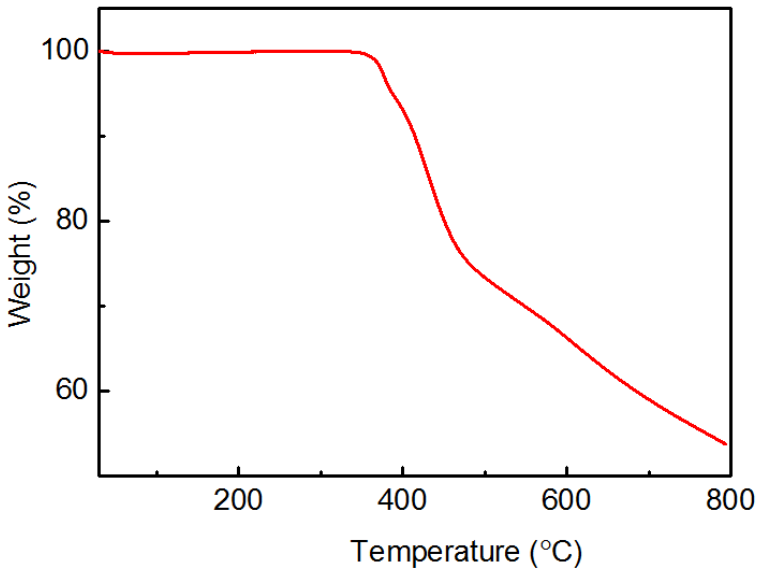

Figure S9. TGA curve of activated HOF-76a.

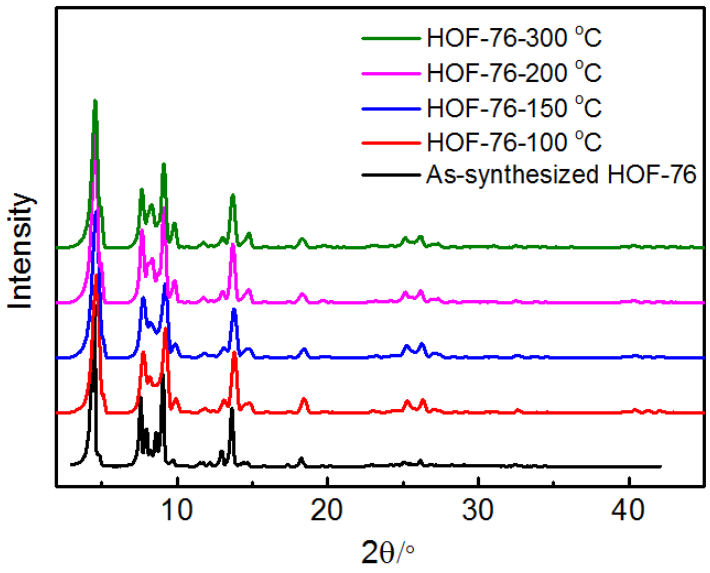

Figure S10. PXRD patterns of HOF-76 sample treated with different temperatures for 2 hours, and compared with the XRD patterns of the as-synthesized sample (black).

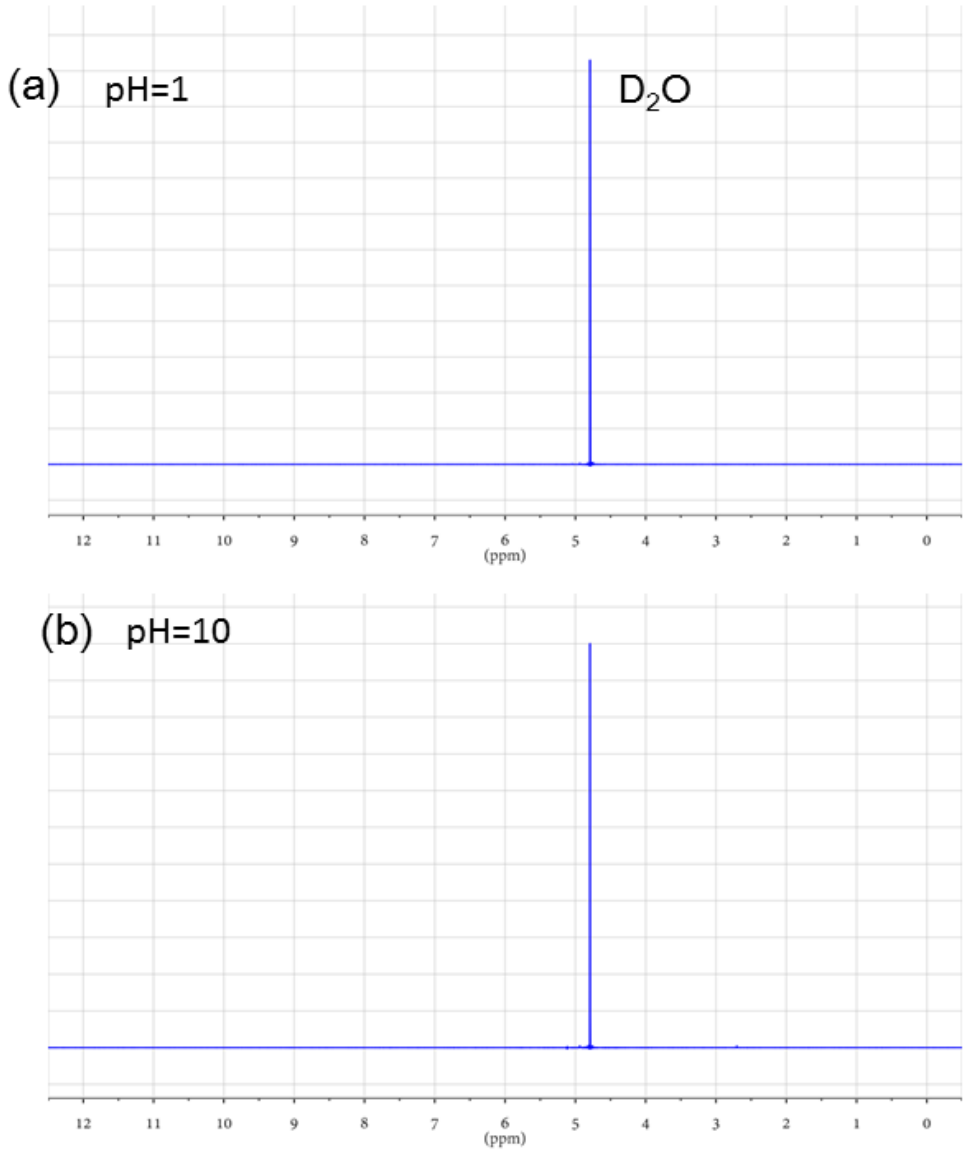

Figure S11. ^{1}H NMR (D_2O, 400 MHz) spectrum of the D_2O solution after the HOF-76 sample was soaked into (a) the pH = 1 HCl solution (0.1 mol/L DCl in D_2O solution) and (b) pH = 10 NaOD solution (0.01 mol/L NaOD in D_2O solution) for 24 h, and no any ligand signal was detected.

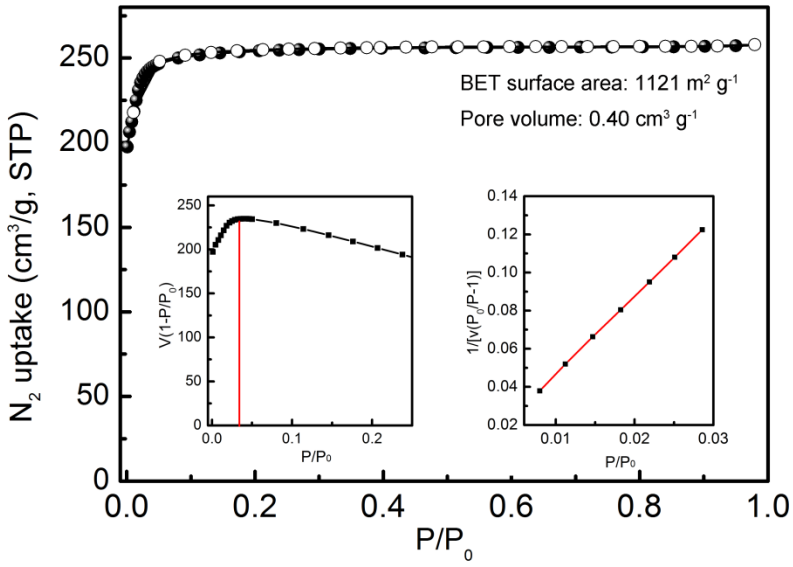

Figure S12. Nitrogen isotherm at 77 K with consistency and BET plots for the activated HOF-76a sample.

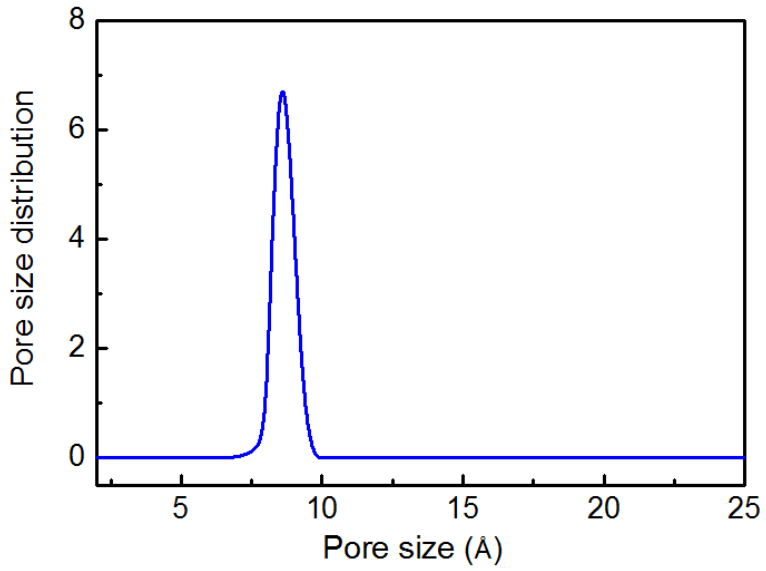

Figure S13. The pore size distribution of HOF-76a determined by 77 K N_2 isotherms using Non Local Density Functional Theory (NLDFT) method, revealing a calculated pore size of 8.5 Å.

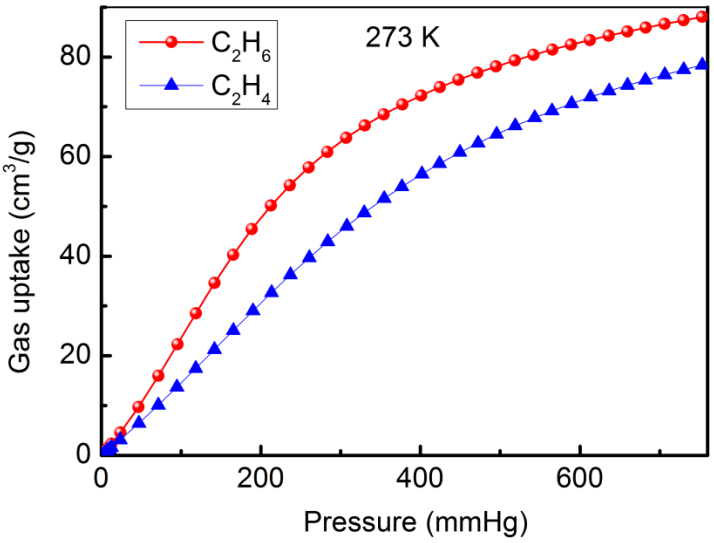

Figure S14. Adsorption isotherms of C_2H_6 (red) and C_2H_4 (blue) for HOF-76a at 273 K up to 1 bar.

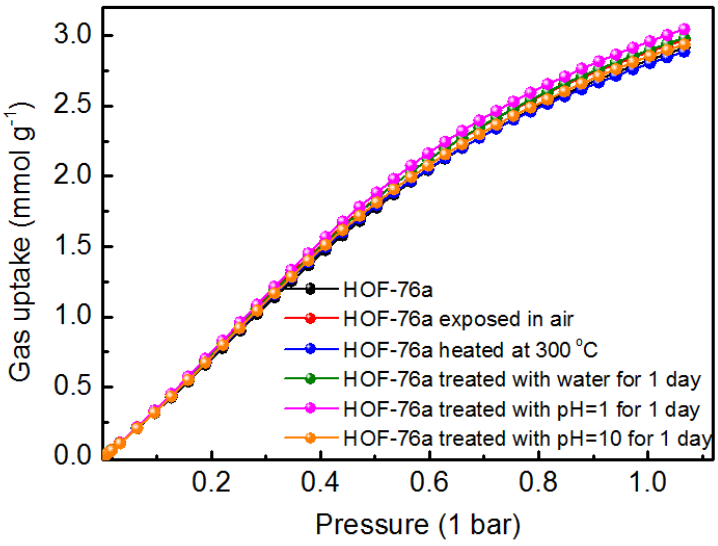

Figure S15. Gas sorption isotherms of C_2H_6 at 296 K for HOF-76a (black), re-activated HOF-76a after exposure to air for 15 days (red), heated at 300 °C for 2 h, and treated with water-, acid- and base-treated HOF-76a.

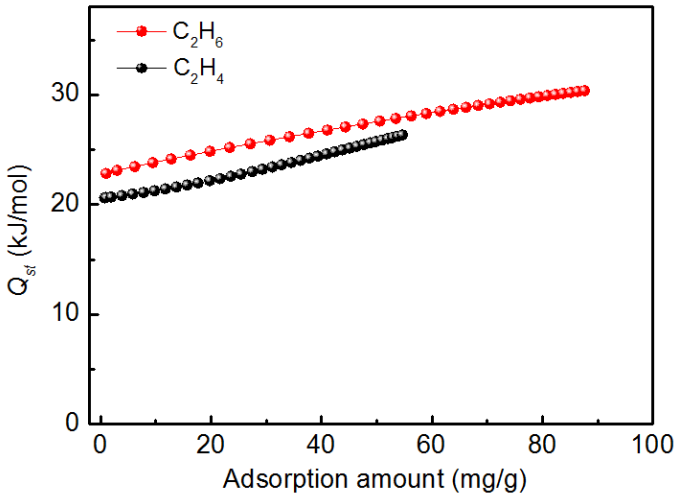

Figure S16. Adsorption heat of the C_2H_6 (red) and C_2H_4 (black) for HOF-76a.

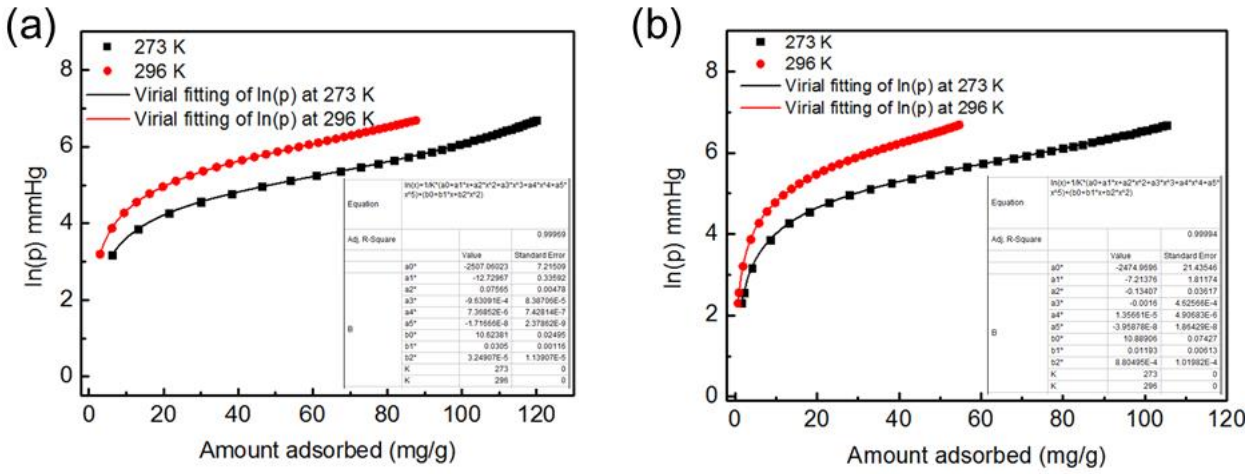

Figure S17. Virial fitting of the C_2H_6 (a) and C_2H_4 (b) adsorption isotherms for HOF-76a.

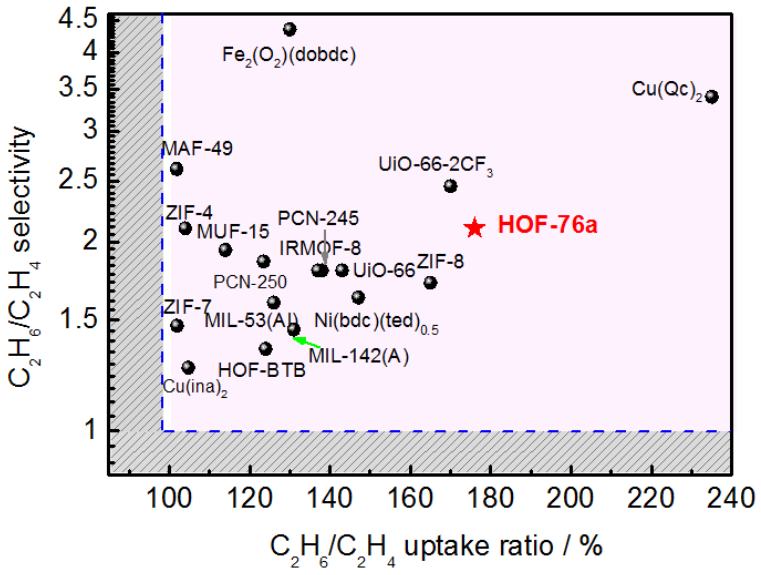

Figure S18. C_2H_6/C_2H_4 IAST selectivity/uptake ratio for HOF-76a (2.05 and 177%) verses the indicated C_2H_6-selective MOF materials at 1 bar and room temperature, indicating that HOF-76a is superior to most of MOFs and the only HOF reported (HOF-BTB: 1.4 and 124%)[23]. HOF-76a is evidently placed among the best-performing materials reported for C_2H_6/C_2H_4 separation.

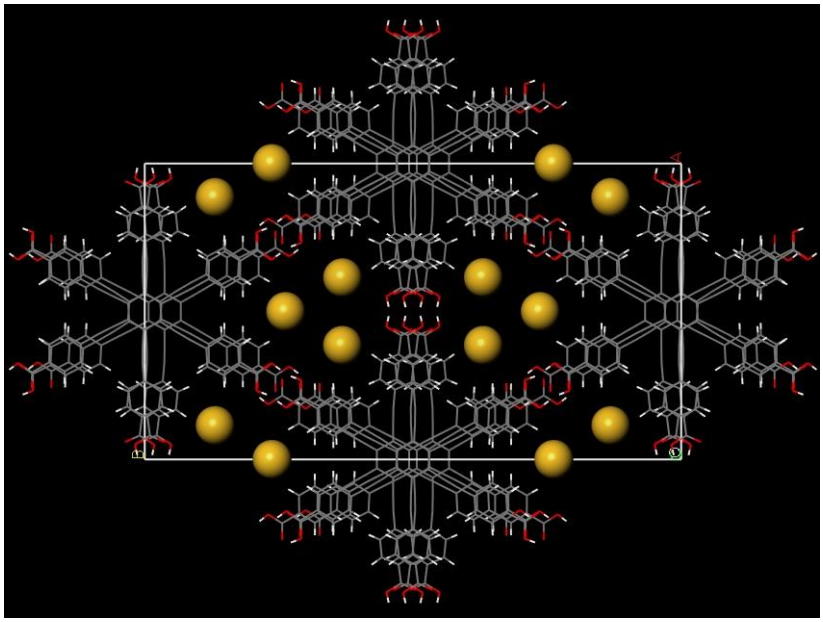

Figure S19. A local structure of HOF-76a showing all the corner sites (yellow ball) for gas adsorption, and there exist 24 such "corner sites" within each unit cell.

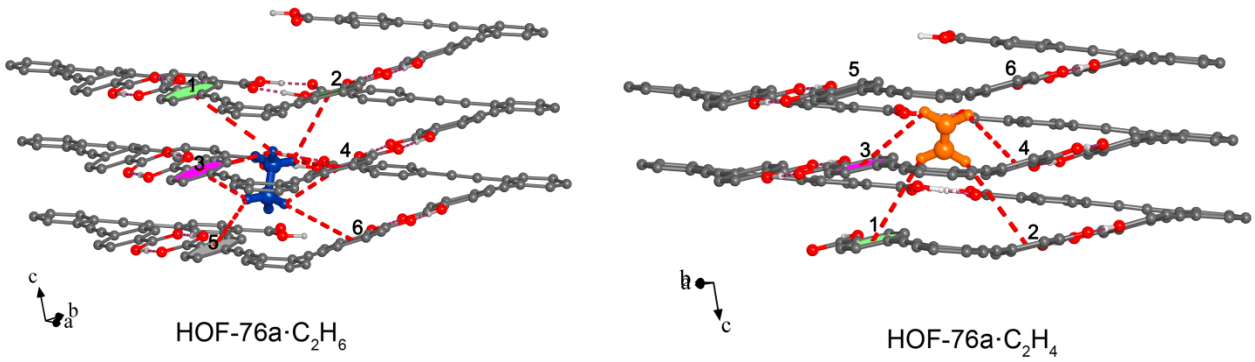

Figure S20. Comparison of the preferential C_2H_4 and C_2H_6 adsorption sites and the close vdW contacts within the corner surface of triangular channel-like pores observed by DFT calculations (C, dark gray; O, red; H, white), highlighting the C−H···π interactions in red dashed bonds.

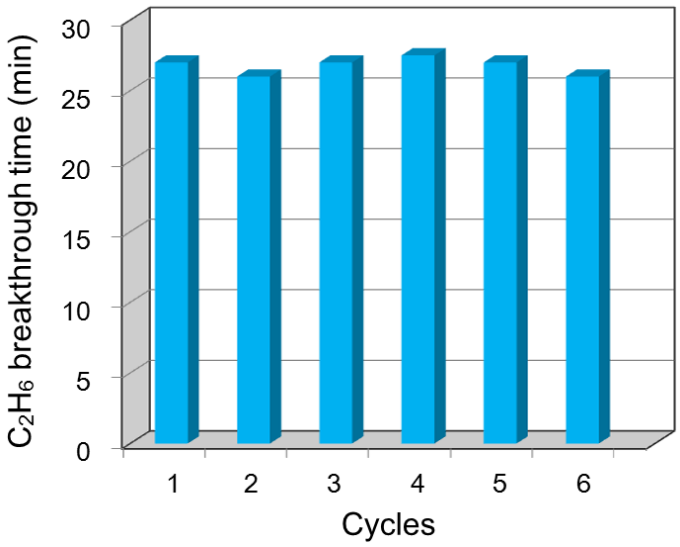

Figure S21. Cyclic breakthrough experiments for C_2H_6/C_2H_4 (50/50) separation on HOF-76a, indicating that HOF-76a maintained the C_2H_6 breakthrough time during the separation processes over at least 6 times.

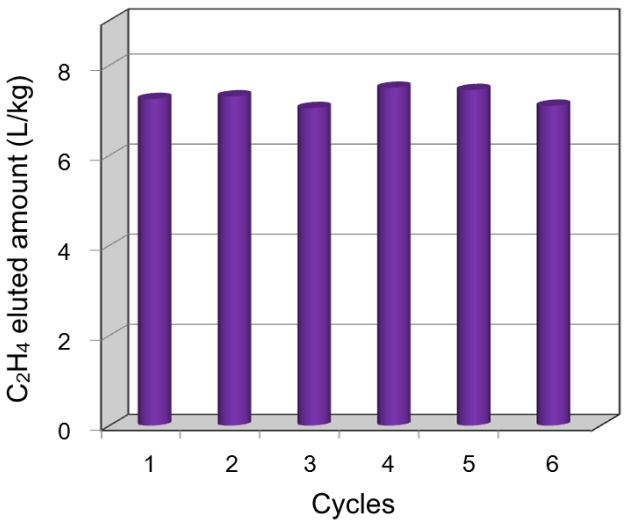

Figure S22. Cyclic breakthrough experiments for C_2H_6/C_2H_4 (50/50) separation on HOF-76a, indicating that HOF-76a maintained the C_2H_4 eluted amount during the separation processes over at least 6 times.

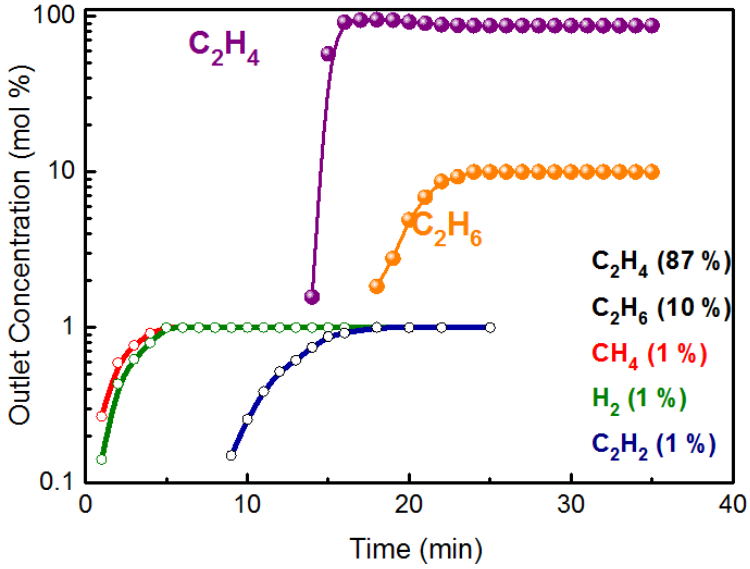

Figure S23. Experimental column breakthrough curves for a $C_2H_6/C_2H_4/C_2H_2/CH_4/H_2$ (10/87/1/1/1) mixture under a total flow of 1.25 mL min^{-1} in an absorber bed packed with HOF-76a at 298 K and 1.01 bar.

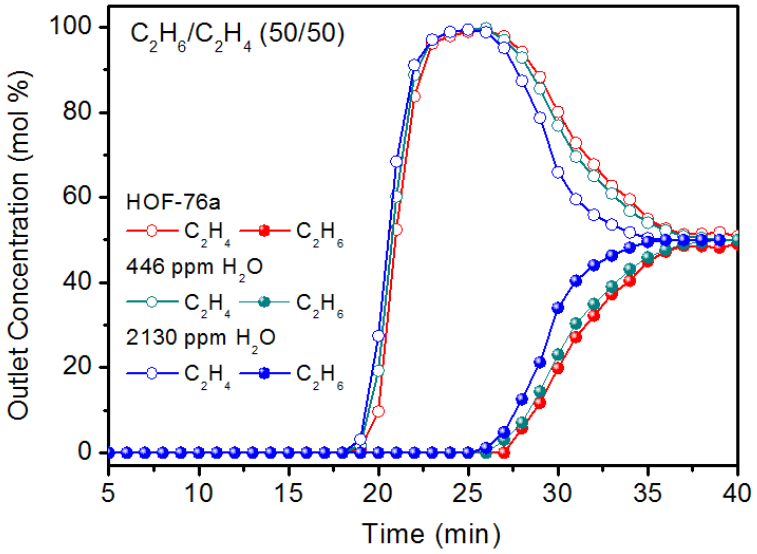

Figure S24. Experimental column breakthrough curves for C_2H_6/C_2H_4 separations (50/50, v/v) on HOF-76a at 298 K and 1.01 bar with different amounts of H_2O, indicating that small amounts of water have a negligible effect on the separation performance.

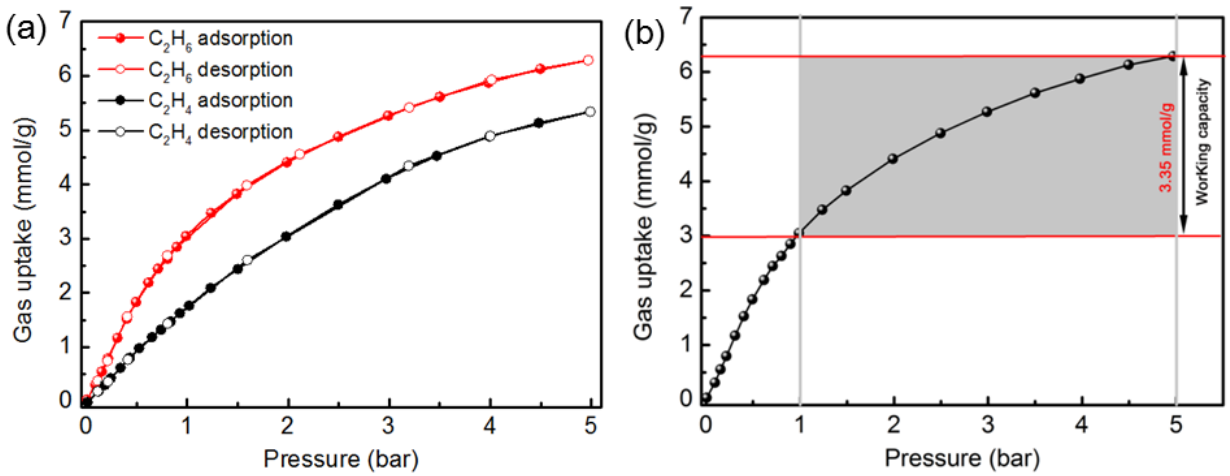

Figure S25. (a) Adsorption isotherms of C_2H_6 (red) and C_2H_4 (black) for HOF-76a at 298 K up to 5 bar. (b) Schematic diagram of the determination of the working capacity of HOF-76a at RT, as required by pressure-swing adsorption (PSA) processes. Here the working capacity is defined as the different amounts adsorbed between 1 and 5 bar, if a PSA regeneration step is considered at near-ambient pressure (≈100 kPa).[14]

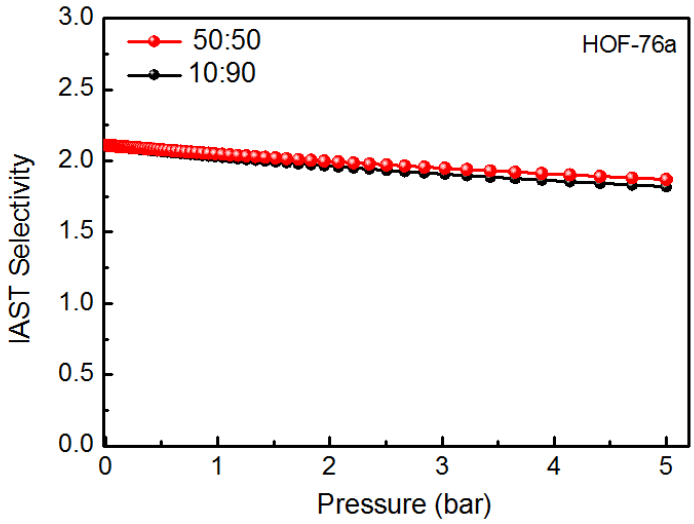

Figure S26. IAST selectivity of HOF-76a from C_2H_6/C_2H_4 (50/50 and 10/90) gas mixtures up to 5 bar, calculated on C_2H_6 and C_2H_4 high-pressure adsorption isotherms at 298 K.

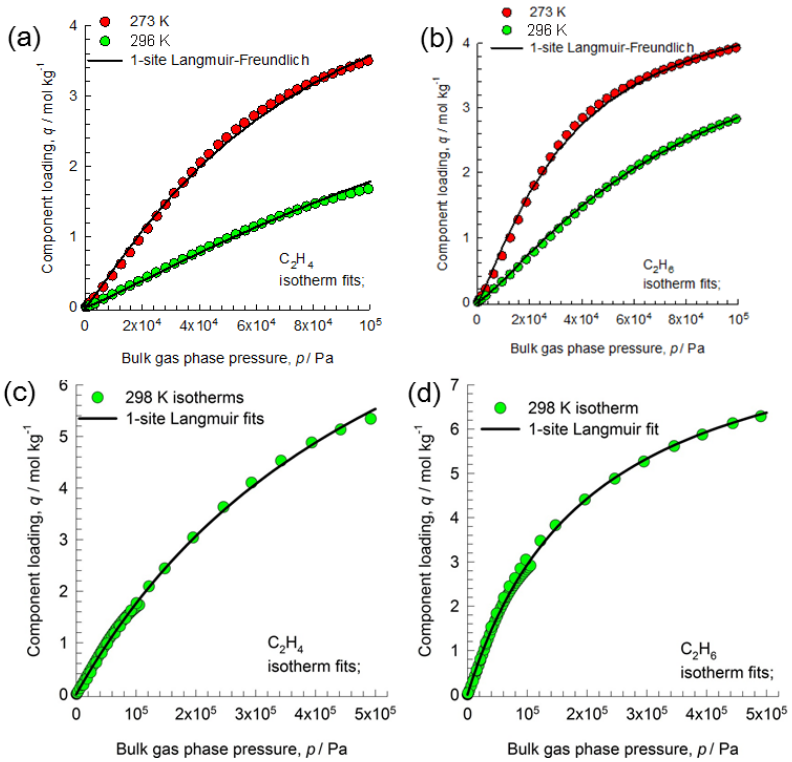

Figure S27. (a) Comparison of component loadings for C_2H_4 and (b) C_2H_6 at 1 bar in HOF-76a with the 1-site Langmuir-Freundlich isotherm fits; (c) for C_2H_4 and (d) C_2H_6 at 5 bar and 298 K.

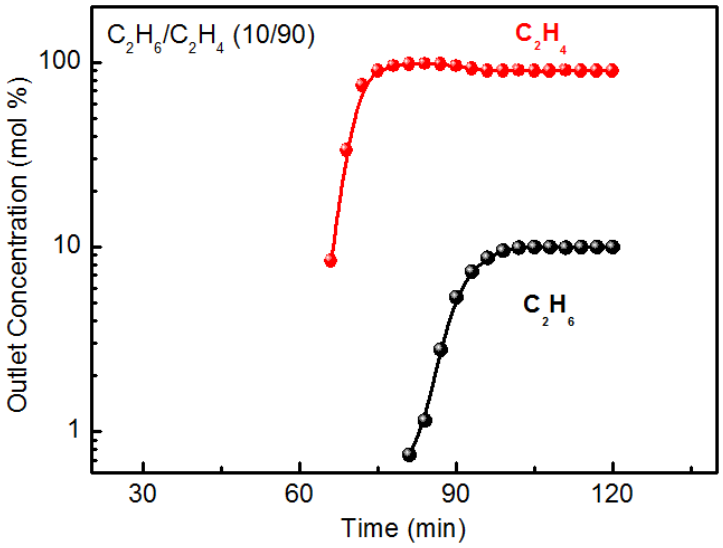

Figure S28. Experimental column breakthrough curves for a C_2H_6/C_2H_4 (10/90) mixture in an absorber bed packed with HOF-76a at 298 K and 5.0 bar.

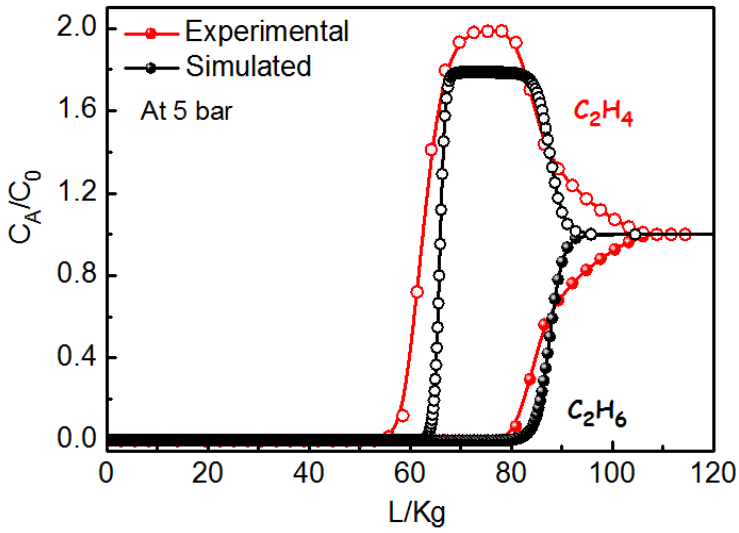

Figure S29. Comparison of the experimental and simulated breakthrough curves for C_2H_6/C_2H_4 separation (50/50, v/v) on HOF-76a under the same separation parameters at 298 K and 5.0 bar, indicating that the simulations are in good agreement with the experimental results. The X-axis represents $\frac{(\text{time in minutes})\times(\text{flow rate mL/min STP})}{(\text{g MOF packed in tube})} = \text{mL}/g$.

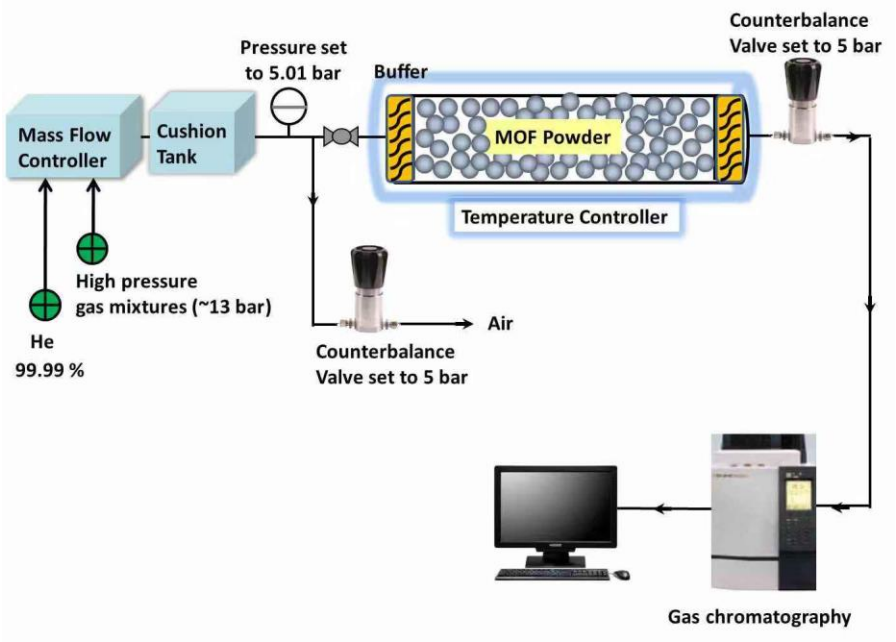

Figure S30. Schematic illustration of the apparatus for the high-pressure breakthrough experiments.

REFERENCES

[1] Krishna, R. Screening Metal-Organic Frameworks for Mixture Separations in Fixed-Bed Adsorbers using a Combined Selectivity/Capacity Metric. *RSC Adv*. **2017**, *7*, 35724–35737.

[2] Krishna, R. Methodologies for Screening and Selection of Crystalline Microporous Materials in Mixture Separations. *Sep. Purif. Technol.* **2018**, *194*, 281–300.

[3] Hu, F.; Liu, C.; Wu, M.; Pang, J.; Jiang, F.; Yuan, D.; Hong, M. An Ultrastable and Easily Regenerated Hydrogen-Bonded Organic Molecular Framework with Permanent Porosity. *Angew. Chem. Int. Ed.* **2017**, *56*, 2101–2104.

[4] Yin, Q.; Zhao, P.; Sa, R.-J.; Chen, G.-C.; Lg, J.; Liu, T.-F.; Cao, R. An Ultra-Robust and Crystalline Redeemable Hydrogen-Bonded Organic Framework for Synergistic Chemo-Photodynamic Therapy. *Angew. Chem. Int. Ed.* **2018**, *57*, 7691–7696.

[5] Hisaki, I.; Nakagawa, S.; Ikenaka, N.; Imamura, Y.; Katouda, M.; Tashiro, M.; Tsuchida, H.; Ogoshi, T.; Sato, H.; Tohnai, N.; Miyata, M. A Series of Layered Assemblies of Hydrogen-

Bonded, Hexagonal Networks of C_3-Symmetric π-Conjugated Molecules: A Potential Motif of Porous Organic Materials. *J. Am. Chem. Soc.* **2016**, *138*, 6617−6628.

[6] Li, P.; Li, P.; Ryder, M. R.; Liu, Z.; Stern, C. L.; Farha, O. K.; Stoddart, J. F. Interpenetration Isomerism in Triptycene-Based Hydrogen-Bonded Organic Frameworks. *Angew. Chem. Int. Ed.* **2019**, *58*, 1664–1669.

[7] Yoon, T.-U.; Baek, S. B.; Kim, D.; Kim, E.-J.; Lee, W.-G.; Singh, B. K.; Lah, M. S.; Bae, Y.-S.; Kim, K. S. Efficient separation of C_2 hydrocarbons in a permanently porous hydrogen-bonded organic framework. *Chem. Commun.* **2018**, *54*, 9360–9363.

[8] Nandi, S.; Chakraborty, D.; Vaidhyanathan, R. A permanently porous single molecule H-bonded organic framework for selective CO_2 capture. *Chem. Commun.* **2016**, *52*, 7249–7252.

[9] Bassanetti, I.; Bracco, S.; Comotti, A.; Negroni, M.; Bezuidenhout, C.; Canossa, S.; Mazzeo, P. P.; Marchió, L.; Sozzani, P. Flexible porous molecular materials responsive to CO_2, CH_4 and Xe stimuli. *J. Mater. Chem. A* **2018**, *6*, 14231–14239.

[10] Li, L.; Lin, R.-B.; Krishna, R.; Li, H.; Xiang, S.; Wu, H.; Li, J.; Zhou, W.; Chen, B. Ethane/ethylene separation in a metal-organic framework with iron-peroxo sites. *Science* **2018**, *362*, 443−446.

[11] Qazvini, O. T.; Babarao, R.; Shi, Z.-L.; Zhang, Y.-B.; Telfer, S. G. A Robust Ethane-Trapping Metal−Organic Framework with a High Capacity for Ethylene Purification. *J. Am. Chem. Soc.* **2019**, *141*, 5014−5020.

[12] Liao, P. Q.; Zhang, W. X.; Zhang, J. P.; Chen, X. M. Efficient purification of ethene by an ethane-trapping metal-organic framework. *Nat. Commun.* **2015**, *6*, 8697.

[13] Lin, R.-B.; Wu, H.; Li, L.; Tang, X.-L.; Li, Z.; Gao, J.; Cui, H.; Zhou, W.; Chen, B. Boosting ethane/ethylene separation within isoreticular ultramicroporous metal-organic frameworks. *J. Am. Chem. Soc.* **2018**, *140*, 12940−12946.

[14] Pires, J.; Fernandes, J.; Dedecker, K.; Gomes, J. R. B.; Pérez-Sánchez, G.; Nouar, F.; Serre, C.; Pinto, M. L. Enhancement of ethane selectivity in ethane-ethylene mixtures by perfluoro

groups in Zr-based metal-organic frameworks. *ACS Appl. Mater. Interfaces* **2019**, *11*, 27410–27421.

[15] Chen, Y.; Qiao, Z.; Wu, H.; Lv, D.; Shi, R.; Xia, Q.; Zhou, J.; Li, Z. An ethane-trapping MOF PCN-250 for highly selective adsorption of ethane over ethylene. *Chem. Eng. Sci.* **2018**, *175*, 110−117.

[16] Lv, D.; Shi, R.; Chen, Y.; Wu, Y.; Wu, H.; Xi, H.; Xia, Q.; Li, Z. Selective Adsorption of Ethane over Ethylene in PCN-245: Impacts of Interpenetrated Adsorbent. *ACS Appl. Mater. Interfaces* **2018**, *10*, 8366−8373.

[17] Liang, W.; Xu, F.; Zhou, X.; Xiao, J.; Xia, Q.; Li, Y.; Li, Z. Ethane selective adsorbent Ni(bdc)(ted)$_{0.5}$ with high uptake and its significance in adsorption separation of ethane and ethylene. *Chem. Eng. Sci.* **2016**, *148*, 275−281.

[18] Ribeiro, R. P. P. L.; Camacho, B. C. R.; Lyubchyk, A.; Esteves, I. A. A. C.; Cruz, F. J. A. L.; Mota, J. P. B. Experimental and computational study of ethane and ethylene adsorption in the MIL-53(Al) metal-organic framework. *Microporous Mesoporous Mater.* **2016**, *230*, 154–165.

[19] Pires, J.; Pinto, M. L.; Saini, V. Ethane selective IRMOF-8 and its significance in ethane-ethylene separation by adsorption. *ACS Appl. Mater. Interfaces* **2014**, *6*, 12093–12099.

[20] Böhme, U.; Barth, B.; Paula, C.; Kuhnt, A.; Schwieger, W.; Mundstock, A.; Caro, J.; Hartmann, M. Ethene/Ethane and Propene/Propane Separation via the Olefin and Paraffin Selective Metal–Organic Framework Adsorbents CPO-27 and ZIF-8. *Langmuir* **2013**, *29*, 8592−8600.

[21] Gücüyener, C.; van den Bergh, J.; Gascon, J.; Kapteijn, F. Ethane/Ethene Separation Turned on Its Head: Selective Ethane Adsorption on the Metal−Organic Framework ZIF-7 through a Gate-Opening Mechanism. *J. Am. Chem. Soc.* **2010**, *132*, 17704−17706.

[22] Hartmann, M.; Böhme, U.; Hovestadt, M.; Paula, C. Adsorptive separation of olefin/paraffin mixtures with ZIF-4. *Langmuir* **2015**, *31*, 12382−12389.

[23] Yoon, T.-U.; Baek, S. B.; Kim, D.; Kim, E.-J.; Lee, W.-G.; Singh, B. K.; Lah, M. S.; Bae, Y.-S.; Kim, K. S. Efficient separation of C_2 hydrocarbons in a permanently porous hydrogen-bonded organic framework. *Chem. Commun.* **2018**, *54*, 9360−9363.

Disclaimer: Certain commercial suppliers are identified in this paper to foster understanding. Such identification does not imply recommendation or endorsement by the National Institute of Standards and Technology, nor does it imply that the materials or equipment identified are necessarily the best available for the purpose.